



# A semi-Lagrangian view of ozone production tendency in North American outflow in the summers of 2009 and 2010

B. Zhang<sup>1</sup>, R. C. Owen<sup>1</sup>, J. A. Perlinder<sup>1</sup>, A. Kumar<sup>1</sup>, S. Wu<sup>1</sup>, M. Val Martin<sup>2</sup>, L. Kramer<sup>1</sup>, D. Helmig<sup>3</sup>, and R. E. Honrath<sup>1,†</sup>

<sup>1</sup>Atmospheric Sciences Program, Michigan Technological University, Houghton, MI, USA

<sup>2</sup>Department of Atmospheric Science, Colorado State University, Fort Collins, CO, USA

<sup>3</sup>Institute of Arctic and Alpine Research, University of Colorado, Boulder, CO, USA

†Deceased

Correspondence to: R. C. Owen (rcowen@mtu.edu)

Received: 3 May 2013 – Published in Atmos. Chem. Phys. Discuss.: 10 June 2013

Revised: 18 December 2013 – Accepted: 15 January 2014 – Published: 4 March 2014

**Abstract.** The Pico Mountain Observatory, located at 2225 m a.s.l. in the Azores Islands, was established in 2001 to observe long-range transport from North America to the central North Atlantic. In previous research conducted at the observatory, ozone enhancement ( $> 55 \text{ ppbv}$ ) in North American outflows was observed, and efficient ozone production in these outflows was postulated. This study is focused on determining the causes for high  $d[\text{O}_3]/d[\text{CO}]$  values ( $\sim 1 \text{ ppbv ppbv}^{-1}$ ) observed in the summers of 2009 and 2010. The folded retroplume technique, developed by Owen and Honrath (2009), was applied to combine upwind FLEXPART transport pathways with GEOS-Chem chemical fields. The folded result provides a semi-Lagrangian view of polluted North American outflow in terms of physical properties and chemical processes, including production/loss rate of ozone and  $\text{NO}_x$  produced by lightning and thermal decomposition of peroxy acetyl nitrate (PAN). Two transport events from North America were identified for detailed analysis. High  $d[\text{O}_3]/d[\text{CO}]$  was observed in both events, but due to differing transport mechanisms, ozone production tendency differed between the two. A layer of net ozone production was found at 2 km a.s.l. over the Azores in the first event plume, apparently driven by PAN decomposition during subsidence of air mass in the Azores–Bermuda High. In the second event, net ozone loss occurred during transport in the lower free troposphere, yet observed  $d[\text{O}_3]/d[\text{CO}]$  was high. We estimate that in both events, CO loss through oxidation contributed significantly to  $d[\text{O}_3]/d[\text{CO}]$  enhancement. Thus, it is not appropriate to use CO as a passive tracer of

pollution in these events. In general, use of  $d[\text{O}_3]/d[\text{CO}]$  as an indicator of net ozone production/loss may be invalid for any situation in which oxidants are elevated. Based on our analysis, use of  $d[\text{O}_3]/d[\text{CO}]$  to diagnose ozone enhancement without verifying the assumption of negligible CO loss is not advisable.

## 1 Introduction

Ozone plays key roles in tropospheric chemistry and air quality. Photolysis of ozone is a primary source of the hydroxyl radical, the primary oxidant in the atmosphere (Logan et al., 1981; Thompson., 1981). Anthropogenic activities such as fossil-fuel combustion produce large amounts of ozone precursors (CO, hydrocarbons, and nitrogen oxides) (Mahlman et al., 1980). The photochemical lifetime of ozone in the troposphere ranges from days to weeks (Wang et al., 1998a), while intercontinental transport of air pollution can occur in 4–10 days (Stohl et al., 2002). Intercontinental transport has been found to carry considerable amounts of ozone to downwind continents (e.g., Guerova et al., 2006). Ozone production tendency during transport is controlled by the availability of ozone precursors, with net ozone production having been observed in pollution originating in eastern Asia (Kotchenruther et al., 2001) and North America (e.g., Reeves et al., 2002; Auvray et al., 2007; Hudman et al., 2009).

Production of ozone in remote regions of the troposphere is thought to be limited by available  $\text{NO}_x$  ( $\text{NO} + \text{NO}_2$ ) in the

atmosphere (Chameides et al., 1992).  $\text{NO}_x$  has a relatively short lifetime, less than 24 h (Liu et al., 1987), and can be quickly oxidized to nitric acid ( $\text{HNO}_3$ ) and peroxy acetyl nitrate (PAN). Removal of  $\text{NO}_x$  and total reactive nitrogen ( $\text{NO}_y$ ) is very sensitive to ambient conditions such as temperature and relative humidity (RH). PAN is an important  $\text{NO}_x$  reservoir in the troposphere and has a lifetime of up to several months in the upper troposphere (Kleindienst, 1994), though it can quickly decompose in the marine boundary layer (MBL; lifetime < 2.5 days; Parrish et al., 1992). PAN decomposition has been found to be a potential  $\text{NO}_x$  source, which can lead to ozone production during the transport of pollution plumes (Kotchenruther et al., 2001; Zhang et al., 2008; Fischer et al., 2011).

Meteorological conditions during pollution export and transport are thought to be critical to the deposition of ozone precursors and ozone production tendency. Air masses can be exported from the continental boundary layer (CBL) by lifting into the free troposphere (FT, 3–4 km a.s.l.), where air masses are transported by strong geostrophic winds. Export of air pollution from populated areas can also occur close to the boundary layer (< 2–3 km a.s.l.; e.g., Neuman et al., 2006). The meteorological conditions at various altitudes vary, with the troposphere composed of the warm and humid air near the ground and cold and dry at higher altitudes. Thus, detailed meteorological conditions and transport pathways should be considered during studies of ozone production tendency.

Ozone and ozone precursors exported from the North American boundary layer, especially from the populated eastern coastal region, are known to impact air quality over the North Atlantic (Parrish et al., 1993) and even over Europe (Auvray and Bey, 2005). Findings from the North Atlantic Regional Experiment (NARE), a multiyear campaign that began in 1993, suggested anthropogenic emissions contribute significant amounts to the ozone budget in the North Atlantic region (Fehsenfeld et al., 1996). More recently, the International Consortium for Atmospheric Research on Transport and Transformation (ICARTT; Fehsenfeld et al., 2006) study, conducted during July–August 2004, revealed observations indicating high ozone levels (up to 100 ppbv) in North American outflows (Mao et al., 2006). In other measurement periods, only slightly elevated ozone (> 55 ppbv) was observed in the free troposphere near the east coast of the U.S. by using retrievals from the Tropospheric Emission Spectrometer (TES; Hegarty et al., 2009). Despite this body of research, ozone production tendency in North American outflow further downwind is incompletely characterized.

In order to study the photochemical evolution of pollutants in the continental outflows from North America, an observatory was established in July 2001 on top of Mt. Pico in the Azores Islands ( $38.47^\circ \text{N}$ ,  $28.40^\circ \text{W}$ , 2225 m a.s.l.), which enabled frequent sampling of North American outflows following the prevailing westerly winds at midlatitudes. Measurements of ozone and CO at the Pico Mountain Observa-

tory (PMO) demonstrated an influence of long-range transported pollution (Honrath et al., 2004). Periods of elevated ozone were linked to anthropogenic emissions (Owen et al., 2006) and boreal forest fires (Lapina et al., 2006), both of which contribute to enhancement in nitrogen oxides in the central North Atlantic (Val Martin et al., 2008). In this study, we conduct a semi-Lagrangian analysis (Owen and Honrath, 2009) to investigate transformations of chemical species and the associated meteorological conditions during transport. As the first application of this method, we focus on anthropogenic pollution events with relatively simple transport patterns. We present detailed analysis of the chemical evolution of two pollution plumes transported from North America to PMO in the summers of 2009 and 2010. The analysis enables us to evaluate the validity of the assumption that  $d[\text{O}_3]/d[\text{CO}]$  indicates net ozone production/loss during transport.

## 2 Methods

### 2.1 Pico Mountain Observatory and measurements

Summertime measurements of CO,  $\text{O}_3$ ,  $\text{NO}_x$ ,  $\text{NO}_y$ , non-methane hydrocarbons (NMHC), RH, and black carbon were collected in 2009 and 2010 at Pico Mountain Observatory. The observatory is located at an altitude of 2225 m a.s.l., which prevents it from being influenced by local upslope flow for over 80 % of the time in summer (Kleissl et al., 2007), providing a unique land-based location for the observation of free tropospheric air in the North Atlantic.

CO levels were measured using a modified commercial instrument (Thermo Environmental Inc., model 48C-TL). Its sensitivity was calibrated daily with a standard gas that was referenced against the calibration scale of the Global Monitoring Division, NOAA, Boulder, CO. Ozone was measured with two commercial ultraviolet absorption instruments (Thermo Environmental Instruments Inc., model 49C). Honrath et al. (2004) presented details on these methods for CO and ozone measurement. NO,  $\text{NO}_2$ , and  $\text{NO}_y$  were measured using an automated system that was custom developed at Michigan Technological University. NO was detected by  $\text{O}_3$  chemiluminescence,  $\text{NO}_2$  by conversion to NO via ultraviolet photodissociation, and  $\text{NO}_y$  by Au-catalyzed reduction to NO in the presence of CO (Val Martin et al., 2006). In this work, we present 30 min averaged measurement data of summers 2009 and 2010 for all species in Figs. 1 and 2.

### 2.2 Application of FLEXPART

The Lagrangian particle dispersion model (LPDM) FLEXPART (version 8.2; Stohl et al., 1998) was used to simulate transport of North American outflows. Both forward and backward modes were implemented to simulate North American outflows and transport trajectories. CO from the Emissions Database for Global Atmospheric Research (EDGAR

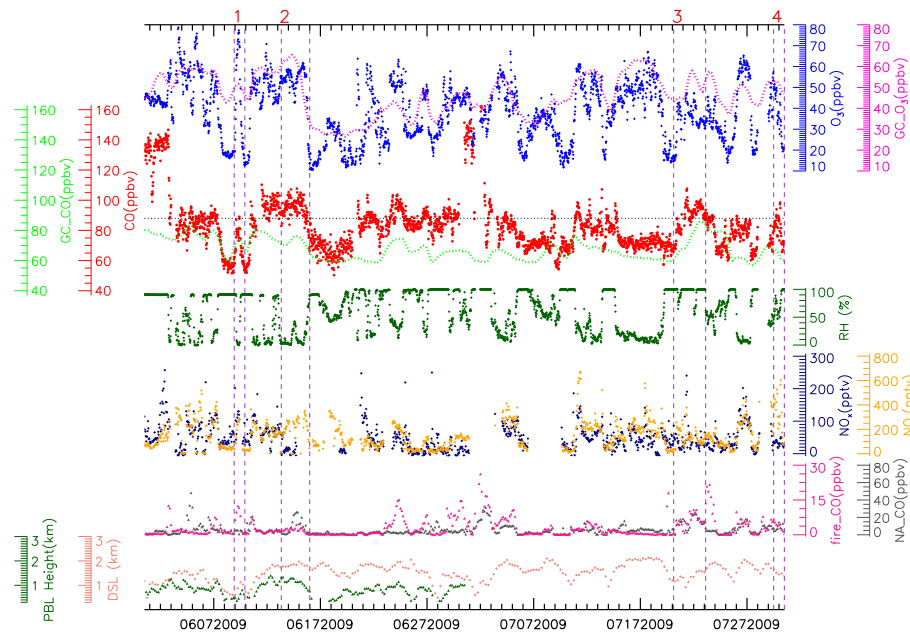


**Fig. 1.** Time series of 30 min average of measurements and meteorological conditions, 6 h average contributions from North American anthropogenic emission (NA\_CO) and biomass burning emissions (FIRE\_CO) calculated by FLEXPART, and 4 h average GEOS-Chem CO (GC\_CO) and O<sub>3</sub> (GC\_O<sub>3</sub>) at Pico Mountain Observatory station during summer 2009. Data points are colored with corresponding y axes. Vertical dashed lines show time windows of each event, which are labeled with red numbers close by at the top.

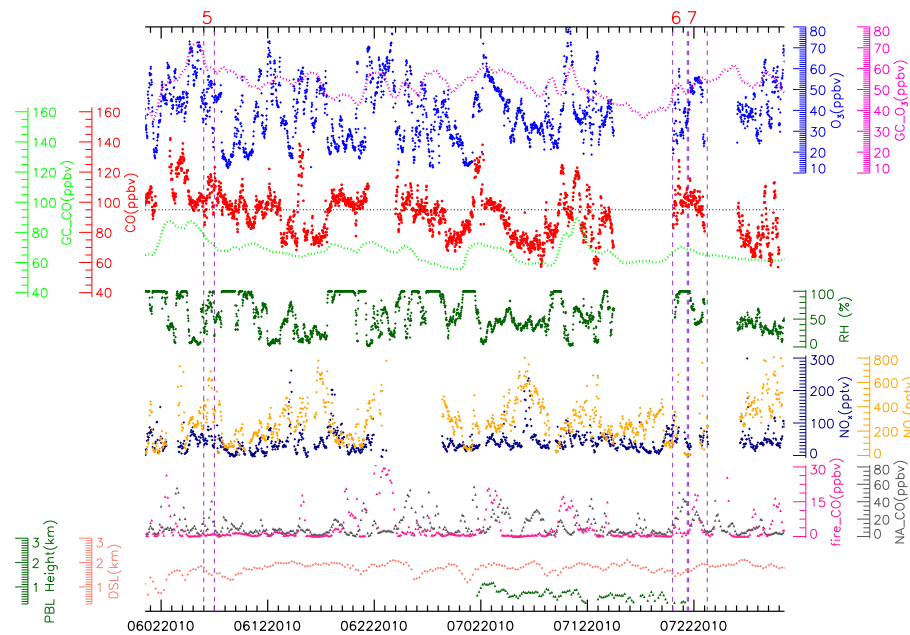


**Fig. 2.** Same as Fig. 1 but for summer 2010.

version 3.2; Olivier and Berdowski, 2001) annually averaged anthropogenic emissions and the Global Fire Emissions Database (GFED v3.1, daily averaged fire emissions; Mu et al., 2011) were used in FLEXPART runs. A combination of 6 h meteorological NCEP Final Analysis (FNL) data at 00:00, 06:00, 12:00, and 18:00 UTC and 6 h Global Forecast

System (GFS) data at 03:00, 09:00, 15:00, and 21:00 UTC was used to drive FLEXPART. The data set had a 3-hourly temporal resolution, with 1 horizontal resolution and 26 vertical levels.

When simulations were conducted in the backward mode, a passive tracer was released from the receptor and advected

and dispersed backwards in time, resulting in spatial distribution of the air mass at an upwind time, referred to as a “retroplume”. The retroplumes can be used to calculate a time series of tracer concentrations at the receptor contributed by a certain emission source (e.g., anthropogenic or biomass burning) by multiplying the residence time in the lowest 300 m by the emission flux (Seibert and Frank, 2004). In this study, backward simulations were set in two different spatial resolutions. For the purpose of identification of North American transport events, retroplumes were released every 3 h, with 4000 particles released over a 1 h time interval from a  $1^\circ \times 1^\circ$  horizontal grid box of altitude from 2000 to 2500 m a.s.l. centered at PMO. The retroplume output was saved in a grid with a  $1^\circ \times 1^\circ$  horizontal resolution in 11 vertical levels from 300 to 15 000 m a.s.l. A high-resolution retroplume simulation, in which 10 000 particles were released every 3 h, was conducted for higher accuracy in the folded GEOS-Chem and FLEXPART technique (see below). FLEXPART output in this high-resolution run was saved in a grid with a  $2^\circ$  (latitude)  $\times 2.5^\circ$  (longitude) horizontal resolution in 130 vertical levels from 0 to 8 km a.s.l.

Forward simulations injected anthropogenic CO emissions into the lowest 300 m over North America. Two forward simulations were conducted: one with EDGAR anthropogenic CO emissions in an output grid matching the retroplume grid used as a component of folded FLEXPART retroplume analysis (see Sect. 2.4), and one with emissions from the same inventory used in GEOS-Chem simulations and with the same grid, used to evaluate discrepancies in transport between FLEXPART and GEOS-Chem (see Sect. 3.3).

### 2.3 Application of GEOS-Chem

GEOS-Chem is a global three-dimensional model of tropospheric chemistry driven by assimilated meteorological observation fields from the Goddard Earth Observing System (GEOS) of the NASA Global Modeling Assimilation Office (Bey et al., 2001). The model has fully coupled ozone– $\text{NO}_x$ –VOC–aerosol chemistry, and can resolve more than 120 species with a sparse matrix vector gear code chemical solver (Jacobson and Turco, 1994). Anthropogenic emissions in GEOS-Chem follow the EDGAR global inventory (Olivier and Berdowski, 2001) and are updated with regional inventories including the U.S. Environmental Protection Agency National Emissions Inventory (EPA/NEI05 and EPA/NEI99), Environment Canada’s Criteria Air Contaminants inventory, the European Monitoring and Evaluation Programme inventory, and the STREETS Emission Inventory in Asia (Streets et al., 2003). The GEOS-Chem model has been extensively evaluated and applied to a wide range of research topics related to atmospheric chemistry and air quality (e.g., Martin et al., 2002; Evans and Jacob, 2005; Duncan et al., 2007; Hudman et al., 2007; Wu et al., 2007; Huang et al., 2013). The performance of the model in simulating CO and ozone has been comprehensively evaluated (e.g., Bey et al., 2001;

Wang et al., 2009; Kumar et al., 2013). Simulation of CO was found to be significantly affected by emission inventories used, but model results generally show reasonable agreement with data from various observational sites or networks around the world (Duncan et al., 2007). GEOS-Chem has also been applied to simulate outflow events from North America (Liang et al., 1998; Li et al., 2004; Auvray and Bey, 2005; Hudman et al., 2009). Li et al. (2005) used GEOS-Chem to characterize the major outflow pathways from North America to the North Atlantic, and the model successfully captured ozone chemistry during convective lifting of pollution plumes. In the work by Millet et al. (2006), GEOS-Chem was used to estimate CO in outflows from the U.S. to Chebogue Point.

This study used GEOS-Chem v9-01-02 driven by GEOS-5 meteorology with a horizontal resolution of  $2^\circ \times 2.5^\circ$  and 47 vertical layers. Model simulations for the period of January–July for both 2009 and 2010 are conducted and the results for June 2009 and July 2010 are used in the final analysis. The time steps used for emissions (30 min), chemistry (30 min), transport (15 min), and convection (15 min) are typical of a  $2^\circ \times 2.5^\circ$  simulation. A domain extending from 100 to  $20^\circ$  W (longitude) and 24 to  $56^\circ$  N (latitude) was selected, which includes part of North America and PMO. Instantaneous mixing ratios of relevant tracers (e.g., CO,  $\text{O}_3$ , nitrogen-containing species such as  $\text{NO}_x$  and PAN, and NMHC such as ethane, propane, and propene) with 2 h resolution and diagnostics for meteorology including RH, temperature, and boundary layer height were archived for this domain. In addition, the daily average production/loss rates of  $\text{O}_3$  for June 2009 and July 2010 were saved. These GEOS-Chem simulations are a subset of those used in Kumar et al. (2013), in which the observed CO and ozone trends at PMO were compared with both GEOS-Chem simulations and satellite data from the Atmospheric Infrared Sounder (AIRS) and TES. They found that GEOS-Chem underestimated CO over the North Atlantic, but successfully captured the seasonal cycles and decreasing trends of CO and ozone at PMO.

A tagged CO simulation in GEOS-Chem was also employed in order to study the transport of CO from the U.S. to PMO. A description of this simulation can be found in Duncan et al. (2007). Two-hourly instantaneous tracer mixing ratios for June 2009 and July 2010 were archived for the above domain.

### 2.4 Folded GEOS-Chem and FLEXPART technique

A LPDM retroplume simulates the displacement and deformation of an air mass in the atmosphere. However, LPDMs typically use an Eulerian grid for saving results, and are thus unable to fully describe source-to-receptor transport. To address this issue, Owen and Honrath (2009) derived a method to track pollution plumes by computing the entry-wise product (also known as the Hadamard product; Charles, 1989)

of the output from the forward and backward simulation, a process that has been described as “folding” the two data fields. The output of this method, which we call a folded retroplume, highlights a transport pathway by overlapping forward simulation, initialized at the source, with backward simulation released from the receptor. As a result, a folded retroplume exhibits a 4-D (spatial and temporal) field that contains the polluted air plume and in which most of the physical and chemical processing occurs.

To meet differing objectives, retroplumes can be folded with FLEXPART or GEOS-Chem simulations. FLEXPART retroplumes represent a sensitivity,  $S_{(j,t,(j',t'))}$ , of the air mass in an upwind cell ( $j$ ) at an earlier time ( $t$ ) to that of the entire plume released at the receptor ( $j'$ ) at time  $t'$ . A collection of these sensitivities  $S_{(t,(j',t'))}$  is a 3-D matrix that can be used to estimate the sensitivity of emissions and meteorological conditions from the upwind distribution of the air mass. For time  $t$ , the folded retroplume is obtained by multiplying the sensitivity matrix  $S_{(t,(j',t'))}$  by a quantity matrix  $\chi_t$ . In this study, FLEXPART retroplumes were folded with mixing ratios ( $\chi_t$ ) from FLEXPART forward simulations to produce FLEXPART folded retroplumes (hereafter called “folded retroplumes”). FLEXPART retroplumes were also folded with mixing ratios, ozone reaction rates, and meteorological fields from GEOS-Chem results (hereafter called “folded results”). The former simulate transport pathways, while the latter, as described below, simulate chemical transformation during transport.

The formulation of the folded results can be summarized as follows by using a tracer mixing ratio as an example of the quantity matrix  $\chi_t$ . The retroplume is folded with the GEOS-Chem mixing ratio matrix field  $\chi_{(j,t)}$  of a given species at a specified upwind time. The product, called the partial folded quantity ( $PFQ_{(j,t,(j',t'))}$ ) and calculated in Eq. (1), represents the contribution from the grid cell ( $j$ ) to the mixing ratio of the species in the plume, whereas the distribution of the  $PFQ_{(j,t,(j',t'))}$  at time  $t$  represents the spatial distribution of contributions from all grid cells in the model domain.

$$PFQ_{j,t,(j',t')} = S_{j,t,(j',t')} \cdot \chi_{j,t,(j',t')} \quad (1)$$

A summation of the PFQs over the model domain ( $j$ ) at an upwind time ( $t$ ) measures the mixing ratio of target tracer substance in the entire dispersed plume (Eq. 2), called the upwind folded quantity (UFQ):

$$UFQ_{t,(j',t')} = \sum_j PFQ_{j,t,(j',t')} \quad (2)$$

Variation in UFQ in the target plume changes according to chemical and physical processes simulated by GEOS-Chem. Therefore, chemical transformation in the plume can be simulated by a time series of UFQs and provides a semi-Lagrangian view of plume aging during the transport. This semi-Lagrangian approach uses backward FLEXPART simulation results to sample air masses in an Eulerian GEOS-

Chem field. There are three features of this method that prevent it from providing a perfect Lagrangian view. The fundamental aspect is the difference in meteorology fields driving the two models. GEOS-Chem uses the GEOS meteorology fields, while FLEXPART is driven by GFS fields. Although both GEOS and GFS are considered to be valid simulations of meteorology, some degree of discrepancy is expected between them. The second feature is the result of random components in the models, including turbulence and convection mechanics, which were noted when the method was first published (Owen and Honrath, 2009). Finally, inherent numerical diffusion in GEOS-Chem can lead to extra dilution of pollution plumes. This last issue can be reduced by using higher-resolution simulations but cannot be entirely avoided. Given the large scale of the particular events that met our criteria ( $10^{\circ}\text{lat.} \times 10^{\circ}\text{long.}$ ), the folded results are still able to adequately reflect a Lagrangian view of chemical processing. However, some chemical species in the plume may deviate from mass conservation and the magnitude of deviation may vary for differing conditions, e.g., transport types or properties of species. In regard to the affected results, specific issues are discussed as they arise. In this study, UFQs of mixing ratios such as those of ozone and ozone precursors are of primary interest. UFQs of meteorological conditions such as temperature and RH are also calculated for better characterization of simulated processes.

### 3 Characteristics of North American transport events during the summers of 2009 and 2010

In this section we describe several criteria that were used to identify the transport events from North America to PMO during the summers of 2009 and 2010. The objective is to identify transport events predominantly affected by emission sources over the North American continent that exhibit direct and rapid transport from source to PMO with no interference from local sources due to mechanically forced upslope flow. We present measurement and modeling results for the time periods in which transport events occurred, and select events that met the criteria. Table 1 summarizes a list of qualified events that are impacted by biomass burning emission, anthropogenic emission, or both.

#### 3.1 Criteria applied for transport event identification

##### 3.1.1 Elevated CO

CO is a pollutant that is emitted during incomplete combustion from both anthropogenic and biomass burning sources. Due to its low reactivity in the troposphere (lifetime from weeks to months), CO has been used widely as a tracer of pollution (Fishman and Seiler, 1983). Periods with an observed CO mixing ratio above 88 ppbv for 2009 and 95 ppbv for 2010 (horizontal dashed lines in CO panels in Figs. 1 and 2) were considered to be potential transport events. These

**Table 1.** Summary of analysis used to identify events resulting from anthropogenic outflows from North America.

Event	Period <sup>a</sup>	$d[\text{O}_3]/d[\text{CO}]$	$N^{\text{b}}$	Avg-CO (ppbv)	$d[\text{O}_3]/d[\text{CO}] (\text{GC})^{\text{c}}$	GC-CO <sup>d</sup>	BB <sup>e</sup>	Anth. <sup>f</sup>	Origin in U.S. <sup>g</sup>
1	09/06/2009 10– 10/06/2009 10	2.28 ( $R^2 = 0.838$ )	48	69.2	0.82 ( $R^2 = 0.840$ )	yes	yes	no	E Coast
2	13/06/2009 20– 16/06/2009 12	1.37 ( $R^2 = 0.519$ )	126	93.9	3.54 ( $R^2 = 0.436$ )	yes	no	yes	E Coast
3	20/07/2009 15– 23/07/2009 15	0.85 ( $R^2 = 0.431$ )	131	89.0	0.58 ( $R^2 = 0.395$ )	yes	yes	yes	SE Coast
4	30/07/2009 00– 31/07/2009 00	1.29 ( $R^2 = 0.607$ )	48	80.5	0.78 ( $R^2 = 0.948$ )	yes	yes	yes	SE Coast
5	06/06/2010 12– 07/06/2010 12	0.96 ( $R^2 = 0.348$ )	48	104.1	0.78 ( $R^2 = 0.732$ )	yes	no	yes	Florida
6	20/07/2010 12– 21/07/2010 21	0.99 ( $R^2 = 0.744$ )	64	100.8	1.92 ( $R^2 = 0.139$ )	yes	no	yes	SE Coast
7	22/07/2010 00– 23/07/2010 18	1.29 ( $R^2 = 0.379$ )	72	98.6	-1.4 ( $R^2 = 0.790$ )	yes	yes	yes	E Coast

<sup>a</sup> UTC time in DD/MM/YYYY HH, determined by using ozone and CO measurements as described in text;

<sup>b</sup> number of data collected for each event;

<sup>c</sup>  $d[\text{O}_3]/d[\text{CO}]$  simulated by GEOS-Chem at PMO for event period;

<sup>d</sup> CO elevation for event period in GEOS-Chem simulations;

<sup>e</sup> significant impact from biomass burning emission;

<sup>f</sup> significant impact from North American anthropogenic emission;

<sup>g</sup> determined by FLEXPART folded retroplumes.

cutoff values were defined to be 20 ppbv over the summertime background in each respective year, based on the approach used by Honrath et al. (2004). There were periods of several days (e.g., from 11 to 17 June 2009) as well as short time windows of several hours (e.g., on 9 June 2009) during which measured CO exceeded the cutoff value. All periods identified by this criterion were evaluated against additional criteria that are discussed in detail in Sect. 3.2. While CO levels exceeding the cutoff are the primary indicator of the start and end of each event, neighboring time periods with lower CO levels are combined into events based on the assumption that the edge of event plumes contained lower concentration of pollutants due to dilution by background air.

### 3.1.2 $d[\text{O}_3]/d[\text{CO}]$

The change in  $\text{O}_3$  relative to CO, or  $d[\text{O}_3]/d[\text{CO}]$ , has been widely used as a measure of ozone enhancement (e.g., Parrish et al., 1993). The  $d[\text{O}_3]/d[\text{CO}]$  values cited from other studies and reported in our work are calculated by two-sided regression, which accounts for error in both variables in the regression (Ayers, 2001). Significant correlation between CO and ozone was found over eastern North America. A  $d[\text{O}_3]/d[\text{CO}]$  of 0.3 was speculated to represent a uniform characteristic of boundary layer air over eastern North America in summertime (Chin et al., 1994; Cooper et al., 2001). Various values of this ratio from satellite observation and aircraft campaigns have been reported downwind of North American emission regions. At Nova Scotia, Berkowitz et al. (1996) observed transported pollution plumes that originated from urban areas of North America and  $d[\text{O}_3]/d[\text{CO}]$  ranged from 0.19 to 0.30 ( $R^2 > 0.5$ ). Dur-

ing the 1993 summer NARE intensive campaign, a range in  $d[\text{O}_3]/d[\text{CO}]$  from 0.25 to 0.28 was observed over eastern North America and the North Atlantic (Parrish et al., 1993; Daum et al., 1996; Fehsenfeld et al., 1996). In a spring study, Prados et al. (1999) reported a  $d[\text{O}_3]/d[\text{CO}]$  of 0.21 ( $R^2 = 0.19$ ) during intensive aircraft measurements between the U.S. and Bermuda. Zhang et al. (2006) provided a global distribution of the  $\text{O}_3$ –CO correlation in the middle troposphere (618 hPa) for July 2005 from both TES detection and GEOS-Chem simulation. They found a  $d[\text{O}_3]/d[\text{CO}]$  value of  $0.81 \text{ mol mol}^{-1}$  ( $R^2 = 0.28$ ) over the eastern U.S. The value was shown to be consistent with an observation of  $d[\text{O}_3]/d[\text{CO}] = 0.90 \text{ mol mol}^{-1}$ ,  $R^2 = 0.12$ , at 600–650 hPa from the ICARTT aircraft campaign. Hegarty et al. (2009), also using TES data, reported a much smaller springtime  $d[\text{O}_3]/d[\text{CO}]$  of 0.13 ( $R^2 = 0.048$ ) extending from North America out over the Atlantic Ocean for 2005 and 2006. Values of  $d[\text{O}_3]/d[\text{CO}]$  that have been reported in the literature vary from 0.1 to 1, and in most cases,  $R^2$  values are less than 0.5. The cause of the variation in slope and low correlation may be mixing of differently aged air masses from different sources. Different ozone production tendency during transport can lead to differing values of  $d[\text{O}_3]/d[\text{CO}]$  observed at differing times at the same location. Events that qualify for the study presented here were selected based on the condition to have statistically significant correlation between simultaneously observed CO and ozone at the 95 % confidence level. Values of  $d[\text{O}_3]/d[\text{CO}]$  and  $R^2$  for time periods that met the first criterion (CO mixing ratio  $>$  cutoff) and this criterion are included in Table 1.

### 3.1.3 Transport pathway

Simulated transport pathways of pollution plumes were obtained from FLEXPART folded retroplumes, computed as summarized in Sect. 2.4, in which CO was used as a tracer for anthropogenic pollution. For a given event, PFQs of CO were calculated by folding 3-D CO fields from forward simulation with the 3-D residence time matrix from backward simulation such that the folded retroplume (distribution of PFQs) highlighted the transport pathway. We selected transport events characterized by an anthropogenic emission originating in the eastern U.S. and direct transport pathway to the PMO by examining the FLEXPART folded retroplumes. Transport events with complex pathways are difficult to assess due to complicated chemistry and increased dilution. Therefore, we did not include events with transport pathways exhibiting multiple branches or long looping times (i.e., more than a week) over the North Atlantic Ocean to further evaluation in this study.

### 3.1.4 Anthropogenic versus fire emission impacts

In order to focus on anthropogenic events, we distinguished events according to source type. Contributions from anthropogenic and wildfire emissions were calculated by folding FLEXPART retroplumes with separate emission inventory categories as described in Sect. 2.2. Three-hour averages of CO contributions from each source are presented in Figs. 1 and 2. Events that received more than 10 % of the observed CO mixing ratio at PMO from North American anthropogenic or biomass burning emissions were identified as impacted by the respective emission source and displayed with a “yes” flag in Table 1.

### 3.1.5 Upslope flow

Local boundary layer air masses can be carried by upslope flow to PMO and lead to mixing of free tropospheric air with MBL air. Upslope flow occurs through mechanically forced lifting, in which strong synoptic winds are reflected by the mountain slope, or through buoyant forcing, in which the surface air mass is lifted as a result of solar heating. Kleissl et al. (2007) determined the occurrence of upslope flow to be less than 39 % of the days during the summers of 2004 and 2005. During the days when upslope flow occurred, there was no evidence of significant impacts of uplift on measurement of chemicals interested in this study. For summers of 2009 and 2010, we examined the possibility of upslope flow due to mechanical lifting.

When mechanically forced lifting occurs, air masses above the dividing streamline (DSL) can be lifted to the top of the mountain, while air masses below the DSL travel around the mountain. The altitude of the DSL (in the bottom panel in Figs. 1 and 2) is calculated by using the method described by Sheppard (1956) from the wind speed profiles in the meteo-

rological data set driving FLEXPART (GFS and FNL). During time periods when the height of the DSL was less than the MBL height simulated in GEOS-Chem, PMO may have received MBL air. As shown in Figs. 1 and 2, there were a few time periods when the calculated DSL was below the MBL. These time periods were excluded from event selection.

### 3.1.6 Capture of events in GEOS-Chem

A requirement for valid folding results from the two models is that the events are predicted to occur in both FLEXPART and GEOS-Chem as indicated by enhanced CO levels at PMO in both simulations. CO and ozone data, shown in Figs. 1 and 2, were obtained from a  $4^\circ \times 5^\circ$  GEOS-Chem simulation in the work of Weise (2011). Four-hour-averaged mixing ratios were extracted from the grid cell that was centered at PMO. For all events identified using the other criteria summarized in Table 1, GEOS-Chem indicated elevated CO mixing ratio, demonstrating that events identified through measurements at PMO were also captured in GEOS-Chem.

## 3.2 Characteristics of transport plumes and quantified events

The transport conditions that qualified as events as summarized in Table 1 exhibit a wide variety of characteristics. A range in  $d[\text{O}_3]/d[\text{CO}]$  values (from 0.85 to 2.28) was found for the eight events. Our criteria selected events with significant impacts from anthropogenic or biomass burning emissions. In this study, we looked for events in which  $d[\text{O}_3]/d[\text{CO}]$  was close to or greater than 1, a value found previously at PMO in North American outflows (Honrath et al., 2004). The correlation coefficients reported in Table 1 are greater than those reported in the previous studies discussed in Sect. 3.1.2, and similar to the values for events in the previous study by Honrath et al. (2004). Higher correlation coefficient values are observed at PMO because the measurement data used in the regressions were extracted for an individual transport event as identified based on the above criteria.

Figures 1 and 2 show time series measurement data at PMO and model results of CO contributions from North American anthropogenic and biomass burning emissions in the summers of 2009 and 2010, respectively. We found several events linked to anthropogenic and biomass burning emissions. For instance, plumes for events 2 and 6 were dominated by North American anthropogenic emissions, as indicated by FLEXPART North American CO (NA-CO) contributions of 35 and 42 ppbv (Figs. 1 and 2), respectively. Conversely, event 1 was characterized by fire emission influence, as indicated by the FLEXPART biomass burning CO (FIRE-CO) contribution up to 15 ppbv (Fig. 1). There were also periods when both types of emissions contributed significant amounts of CO (e.g., events 4 and 7). Overall, the frequency and magnitude of contribution from

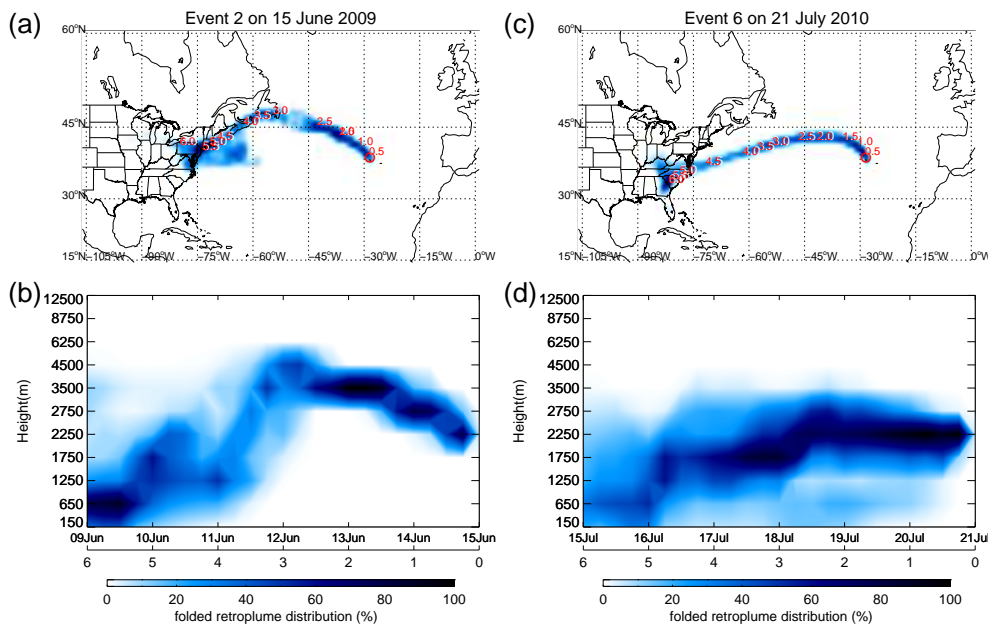


**Fig. 3.** FLEXPART folded retroplumes of events 2 and 6 discussed in text: (a) and (c) are plan views of FLEXPART folded retroplumes with locations at each upwind time labeled by red numbers in days; panels (b) and (d) are vertical distributions of FLEXPART folded retroplumes with dual x-axis labels, showing both date (in UTC) and upwind time. Folded retroplume concentration is shown using a scale normalized to the highest concentration at each upwind time to provide a clearer view of transport pathways.

North American anthropogenic emissions was estimated to be greater than those of biomass burning emissions during the summers of 2009 and 2010. In this study, we examined events 2 and 6 in detail as they meet the criteria described in Sect. 3.1.

### 3.3 Simulation of transport for selected events

Prior to detailed analysis of chemical and physical processes for events 2 and 6, we discuss transport pathways and evaluate the similarity of transport simulation in FLEXPART and GEOS-Chem. The transport characteristics of the two events are discussed in Sect. 3.3.1. As a prerequisite for folding calculation, transport similarity in the two models is evaluated in two approaches. Tagged CO simulations are presented in Sect. 3.3.2 for evaluation of transport similarity in two models from a forward simulation perspective. The coherence of the transport is also examined by analyzing the NMHC photochemical clock in folded results in Sect. 3.3.3.

#### 3.3.1 FLEXPART folded retroplumes

Transport pathways of events 2 and 6 are shown in Fig. 3. The plume associated with event 2 arrived at PMO on 15 June 2009 at 06:00 UTC. At five to four days upwind, the plume was lifted from the planetary boundary layer (PBL) of the northeastern U.S. into the free troposphere (3–4 km a.s.l.) by a warm conveyor belt (WCB) that was identified on NCAR weather maps over the northeastern U.S. (NCAR, 2009). The

plume was then transported from the northeastern U.S. to the central North Atlantic free troposphere, and during this time it was isolated from the MBL air. When approaching PMO, the plume experienced a subsidence from about 4 to 2 km a.s.l. The plume for event 6 originated over the southern U.S. and arrived at PMO on 21 July 2010 at 06:00 UTC. The plume was transported in the lower FT (1.5–2.5 km a.s.l.) to the east-northeast to the North Atlantic without much change in transport altitude (2–3 km a.s.l.).

#### 3.3.2 Tagged CO simulations

One potential source of error in the folding process could be the result of differing transport in FLEXPART and GEOS-Chem simulation. In order to evaluate discrepancies in transport between the two models, forward FLEXPART and GEOS-Chem simulations were conducted for the time periods of events 2 (9–15 June 2009) and 6 (15–21 July 2010) using a tagged CO tracer. The two largest anthropogenic CO emission sources of North America – road transportation and oil production – which comprised approximately 80 % of total CO emissions, were extracted from GEOS-Chem and integrated into a FLEXPART forward simulation. GEOS-Chem seasonal and diurnal variations for these emissions were also taken into account in the FLEXPART simulation. Figure 4 compares results from the forward FLEXPART simulation with a GEOS-Chem tagged CO simulation for event 2.

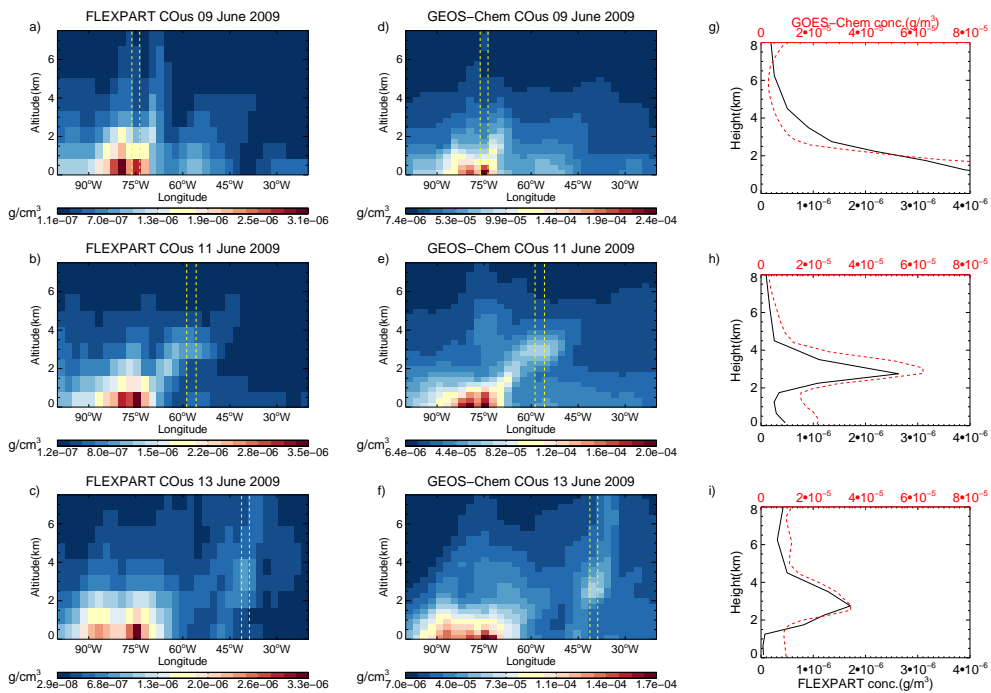


**Fig. 4.** Tagged North American CO simulation results for FLEXPART and GEOS-Chem at three upwind times for event 2: 9 June 2009, 18:00 UTC (upper panel); 11 June 2009, 18:00 UTC (middle panel); and 13 June 2009, 18:00 UTC (lower panel). Concentrations of CO in panels (**a–c**) for FLEXPART and (**d–f**) for GEOS-Chem are averaged along the latitudinal region defined by the model domain (see the text). Panels (**g–i**) present tagged CO profiles from FLEXPART (solid black line) and GEOS-Chem (dashed red line) at the three upwind times with locations determined by maximum CO in folded results (UFQs). The plume locations are also marked with two dashed vertical lines in panels (**a–f**).

Tagged CO simulations demonstrated close agreement between FLEXPART and GEOS-Chem simulation results. Latitudinal averages of North American CO concentrations in FLEXPART (a, b and c) and GEOS-Chem (d, e and f) are shown in three rows in Fig. 4 for three upwind times in which the plume was in the PBL, during lifting, and during transport in the free troposphere, respectively. Similar plumes can be identified in FLEXPART and GEOS-Chem results at all three time steps. Detailed views of CO vertical profiles at the three upwind times (Fig. 4g, h, and i) show that the vertical profiles of CO in FLEXPART and GEOS-Chem agree well at the locations where the plume was predicted. On 9 June, FLEXPART and GEOS-Chem simulations (Fig. 4g) indicate that CO was abundant in the lowest 2 km over the U.S. continental region. On 11 and 13 June, similarity is conserved as the pollution plume was lifted and transported over the North Atlantic (Fig. 4h and i). It is important to note that the concentration of CO simulated in GEOS-Chem was higher than that simulated in FLEXPART, which is caused by discrepancies in emission inventories in the two models and accumulation of long-lived CO during the spin-up period of the GEOS-Chem simulation. The same tagged CO simulations were conducted for event 6; these also exhibit good agreement of transport between the two models (results not shown). The agreement in the two model simulations indi-

cates that the folding technique (Owen and Honrath, 2009) may be used for the analysis.

### 3.3.3 NMHC aging in the folded GEOS-Chem and FLEXPART results

We also evaluated the coherence of the folded results by comparing NMHC aging folded results to theoretical values. Ratios of simultaneously observed NMHC have been used to study photochemical aging of air masses (McKeen and Liu, 1993; Helmig et al., 2008; Honrath et al., 2008). Correlation analysis of natural logarithms of  $[n\text{-butane}]/[\text{ethane}]$  versus  $[\text{propane}]/[\text{ethane}]$  can be used to determine plume age (Parish et al., 1992). If aging of NMHC in the folded results agrees with the theoretical chemical aging rate predicted by GEOS-Chem, we can conclude that the folded results represent a consistent result with the modeled chemical transformation during the transport.

We examined the NMHC aging rate in the folded results and compared it to aging rate predicted based on theoretical decay, as defined by reaction rates in GEOS-Chem for events 2 and 6 (Fig. 5). GEOS-Chem combines mixing ratios of all alkanes having carbon number  $\geq 4$  (ALK4), so ALK4 was used in this analysis of plume aging instead of *n*-butane. A theoretical decay slope (solid blue line in Fig. 5)

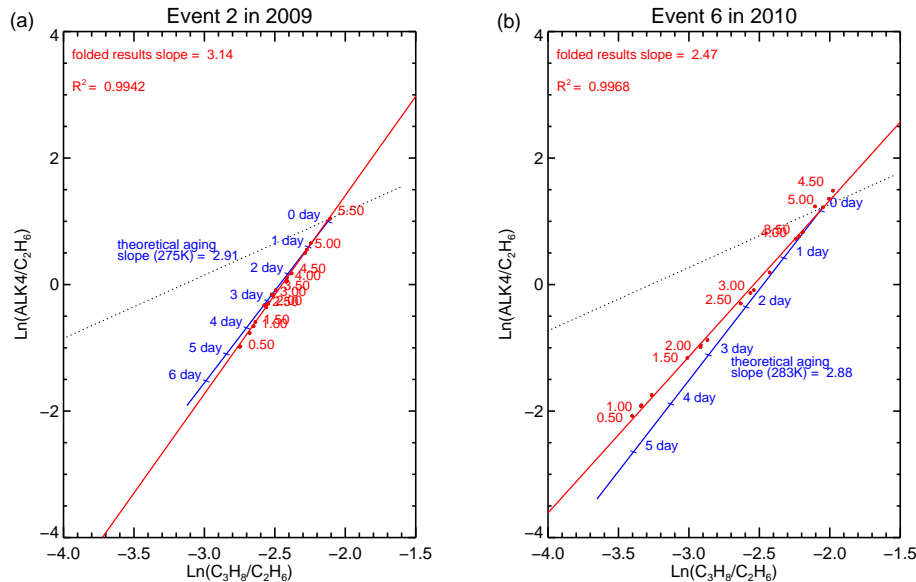


**Fig. 5.** Relationship between the natural logarithms of  $[\text{ALK4}]/[\text{ethane}]$  versus  $[\text{propane}]/[\text{ethane}]$  in folded results during transport of event 2 (a) and event 6 (b). Folded results (UFQs) are shown in red dots, with labels indicating the upwind time at which the simulated data were obtained. Red solid lines indicate the two-sided regressions for folded results, and the slope and  $R^2$  values of the regressions are given in the top-left corner of each plot. The two lines initiating from the youngest data point represent, respectively, mixing of background air containing negligible concentrations of ALK4 and propane (dotted black line) and theoretical oxidation by OH (solid blue line). Marks on the theoretical decay line provide estimates of decay rate at an average ambient temperature in folded results.

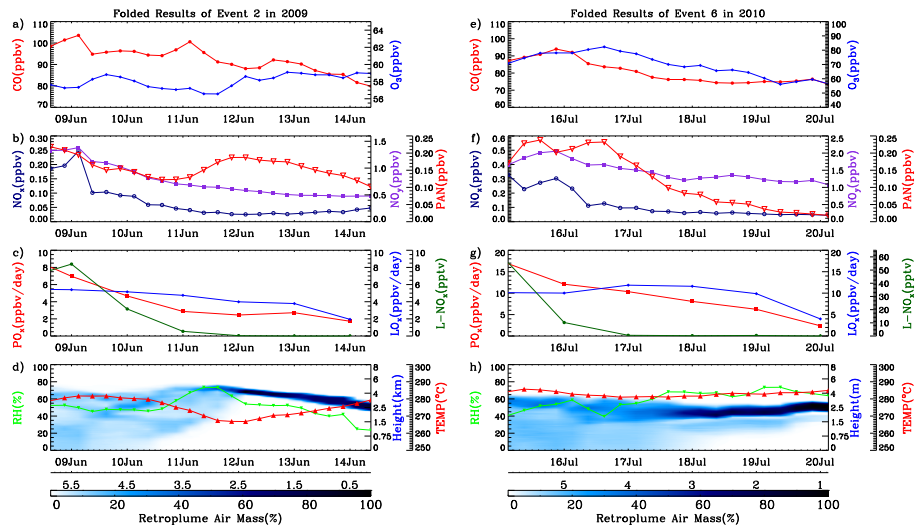


**Fig. 6.** Folded results (UFQs) of pollution plumes at each model time step during event 2 (left column) and 6 (right column). Data color corresponds to the respective  $y$  axes. Six-hour-averaged UFQs of tracer gases are shown in panels (a), (b), (e) and (f). Folded daily averaged UFQs of ozone production ( $PO_x$ ) and loss ( $L-NO_x$ ) rates and lightning  $NO_x$  are shown in panels (c) and (g). FLEXPART retroplume, temperature, and RH in the folded results are shown in panels (d) and (h), with dual  $x$  axes for date in UTC and upwind time in days.

indicates the decay rate of NMHC against the hydroxyl radical, while a mixing line (dotted black line) indicates the trend if the plume mixes with clean background air. Regressions of NMHC UFQs for both events are significant ( $R^2 > 0.9$ ), which suggests that the folded results simulated transport and aging well. If plumes of different ages had been extracted

from GEOS-Chem fields by FLEXPART (indicating discrepancies in transport), folded results of NMHC would deviate from the regression line. Given the similarity in transport observed as discussed in Sect. 3.2, the similarity between the theoretical aging slope and folded results of NMHC in both plumes provides additional evidence that the folding

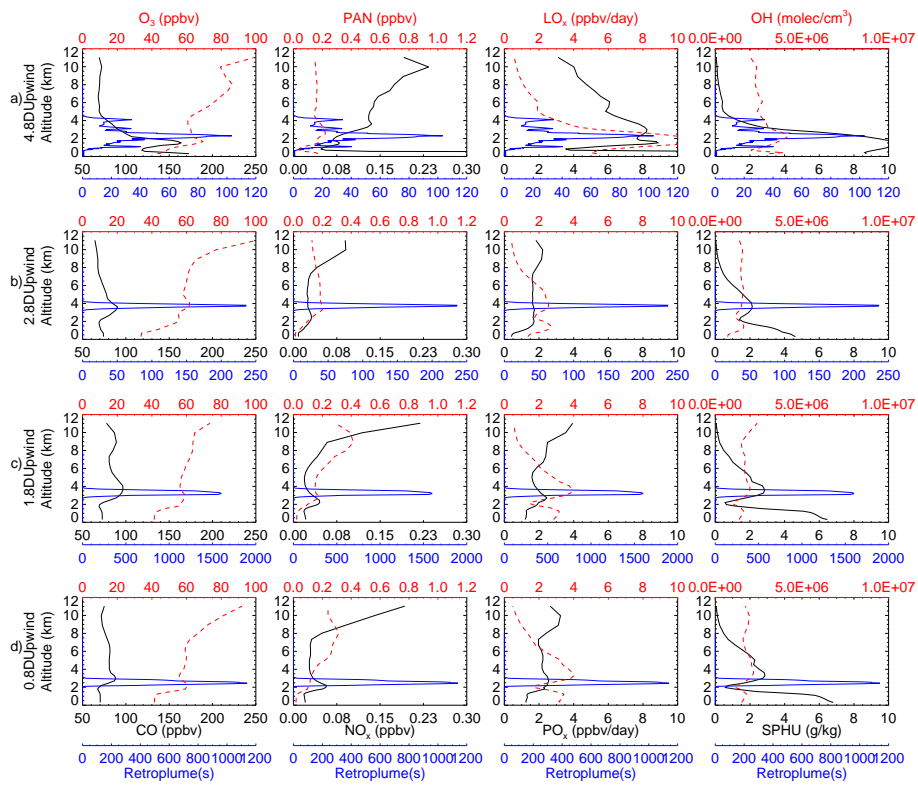


**Fig. 7.** GEOS-Chem profiles of tracer gases ( $\text{CO}$ ,  $\text{O}_3$ ,  $\text{PAN}$ , etc.), ozone production/loss rates ( $\text{PO}_x$ ,  $\text{LO}_x$ ), OH concentration, and specific humidity (SPHU) at four upwind times along the transport pathway for event 2. The four times were selected to show different stages during the transport. Upwind times are indicated to the left of each row. Plume location and altitude are determined by folded retroplume analysis at the indicated upwind time (Fig. 3). Simultaneous retroplumes (in blue) are shown in units of residence time (second), which can be viewed as vertical dispersions of plume air masses over altitude in the column containing the highest folded retroplume concentration such that the retroplume profiles in each row are identical. Each plot shows two GEOS-Chem profiles, the colors of which correspond to the colors of the upper and lower  $x$  axes.

technique performed well in extracting Lagrangian information of the transported plumes from the Eulerian model.

The regression slope for the folded results in event 2 was very close to the theoretical value calculated for reaction with hydroxyl radical only. This may be the result of the transport of a highly compacted plume, as apparent in Fig. 3a. The regression line for event 6 lies between the theoretical decay line and the line for mixing with zero background air, suggesting that the event 6 plume experienced a higher degree of mixing than that of event 2. In each panel shown in Fig. 5, a measure of decay rate for each day is labeled on the theoretical line (blue labels). Theoretical decay rate was computed by substituting the average folded OH level in each plume into the second-order reaction rate equation of the (lumped) alkanes. The decay rates of the folded NMHC results (red labels) and theoretical results (blue labels) are comparable. Distances between the blue labels are greater for the results in event 6 than for those in event 2 because OH levels were higher during transport in event 6 (as it will be shown in Sect. 4), which resulted in relatively faster loss of NMHC. The cause of the higher OH levels estimated for event 6 was

likely the higher exported ozone concentration in the associated plume.

#### 4 Ozone production tendency in North American outflows

In this section we present detailed descriptions of the transport and chemistry that occurred for the two selected events. First, we use the folded GEOS-Chem and FLEXPART retroplume analyses to provide information regarding chemical transformation in the plume during transport (Fig. 6). Second, we use GEOS-Chem profiles to focus on vertical distribution of chemical species at several upwind time frames (Figs. 7 and 8).

##### 4.1 Event 2 (9–15 June 2009)

Figure 6a–d show the time series of folded GEOS-Chem and FLEXPART retroplume results (UFQs) for event 2. These time series include chemistry information during the lifting from the boundary layer, transport in the FT, and start and

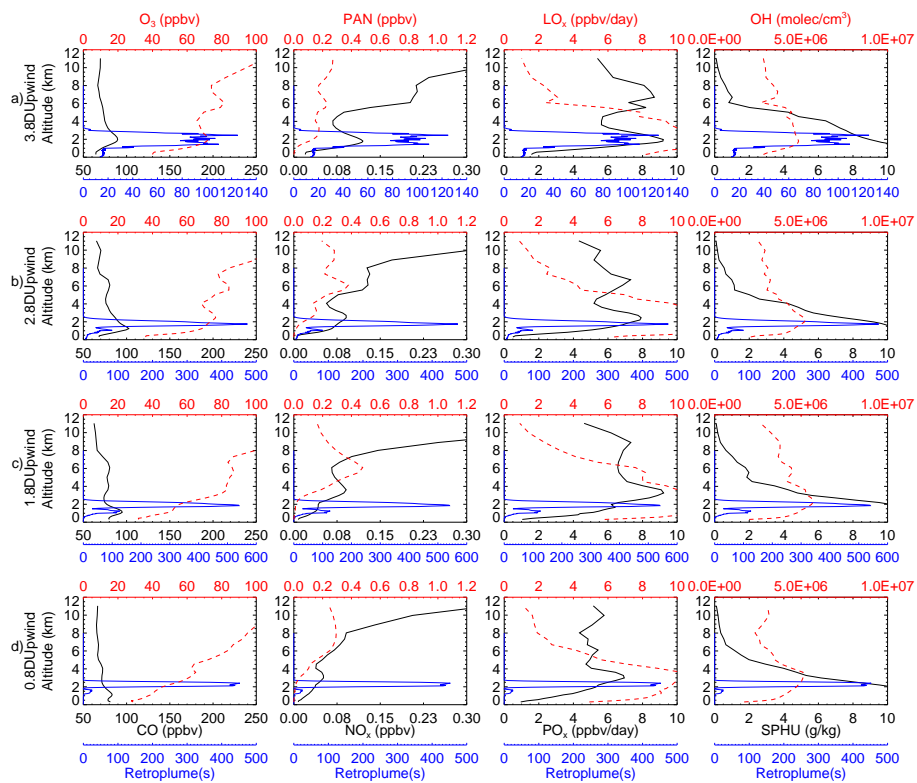


**Fig. 8.** Same format as in Fig. 7 but for event 6 in 2010.

end of the subsidence phase. The FLEXPART retroplume is also shown within the chemical profiles in order to provide reference as to plume shape and altitude at each time shown (Fig. 6d). In addition, Fig. 7 shows profiles of CO, ozone,  $\text{NO}_x$ ,  $\text{NO}_y$ , OH, specific humidity, and production and loss rate of ozone ( $\text{PO}_x/\text{LO}_x$ ) from GEOS-Chem simulation results at 4.8, 2.8, 1.8, and 0.8 days upwind. The profiles are shown at the location of the plume, determined to be the horizontal latitude and longitude of the column with the largest UFQs of CO mixing ratios at the selected upwind times.

The vertical distribution of the FLEXPART retroplume (Fig. 6d) indicates that more than half of the retroplume was distributed in the PBL below 1 km at six days upwind. The retroplume contained high levels of primary pollution species such as CO (> 100 ppbv) and  $\text{NO}_x$  (> 0.2 ppbv) and was in a state of net ozone production ( $2 \text{ ppbv day}^{-1}$ ;  $\text{PO}_x = 7.5$  and  $\text{LO}_x = 5.5 \text{ ppbv day}^{-1}$ ). This net ozone production value is somewhat lower than typical values reported for mid-latitude polluted areas (approximately  $5 \text{ ppbv day}^{-1}$ ; Wang et al., 1998b). However, the lower net production rate is likely due to a lower ozone production rate at higher altitude given that part of the plume extended into the FT.

$\text{NO}_x$  from lightning can be an important contributor to  $\text{O}_3$  production (DeCaria et al., 2005); however, this is not predicted to be the case in this event.  $\text{NO}_x$  from lightning (L- $\text{NO}_x$ ) was estimated to account for a maximum value of

9 pptv of  $\text{NO}_x$  at this time (Fig. 6c), a small fraction (3–5 %) in comparison to the total  $\text{NO}_x$  mixing ratio in the plume (0.18–0.24 ppbv). Thus, lightning  $\text{NO}_x$  was unlikely to contribute significantly to ozone production during this event.

From five to four days upwind, slightly less than 50 % of the retroplume was lifted from the PBL into the FT, and ozone production tendency switched from a state of net production to net destruction (Fig. 6c) because of more efficient loss of  $\text{NO}_x$  than ozone in the pollution plume. In addition, CO mixing ratios dropped slowly as a result of photochemical loss and mixing with background air; levels of oxidized nitrogen species decreased quicker due to relatively shorter photochemical lifetime as compared to CO in the FT. In Fig. 7a, profiles of simulated CO,  $\text{O}_3$ ,  $\text{NO}_x$ , and PAN, as well as production and loss rate of ozone, show maximum values at about 2 km a.s.l. at 4.8 days upwind. This correlation in species concentrations indicates that the pollution plume was concentrated at 2 km a.s.l. at this stage.

Over 80 % of the simulated plume was lifted up into the FT by three days upwind. During the lifting, temperature dropped from 280 K over the continent to 265 K, while RH increased from ~50 to 75 % (Fig. 6d). Oxidized nitrogen species and ozone decreased slightly, which was due to further dilution and destruction, and ozone production tendency remained in a net destruction status at  $-2.2 \text{ ppbv day}^{-1}$  (Fig. 6c). At the same time, PAN levels in the plume

increased from 0.12 to 0.18 ppbv (Fig. 6b). This accumulation of PAN was likely caused by continuous oxidation of  $\text{NO}_x$  to PAN combined with the longer lifetime of PAN in the middle of the FT; the lifetime of PAN is 10–100 times longer in the FT than in the PBL (Kleindienst, 1994). The increase in PAN was found to be much higher than the decrease in  $\text{NO}_x$  during this lifting, which may appear inconsistent if it is assumed that PAN is formed primarily from  $\text{NO}_x$  destruction. When PAN reached its highest mixing ratio at 12:00 UTC on 12 June, due to a slight discrepancy in convection in the two models, the FLEXPART retroplume profile did not entirely match the GEOS-Chem plume profile and only sampled in the upper part of the plume (see Fig. 7, column 1, panel b). During lifting, the GEOS-Chem plume encountered a potential cloud layer (see RH in Fig. 6, panel d). As a consequence, the FLEXPART retroplume, which was concentrated above the potential cloud layer, sampled the upper part of the plume where  $\text{NO}_x$  had already been transformed to PAN or washed out during lifting. The lower part of the plume, where significant  $\text{NO}_x$  change could be expected, was not sampled by the retroplume because of the disagreement in convective transport in the models. Thus, the change in  $\text{NO}_x$  in the folded results may have been underestimated. CO and ozone, which are more stable than  $\text{NO}_x$ , were unaffected by the potential cloud layer on the short timescale, and the retroplume corresponded well to the layers in which CO and ozone were elevated, so the effects on the folded results of CO and ozone were small. After being lifted from the PBL, the plume layer reached an altitude of 3 to 5 km a.s.l., as indicated by the simulated CO profile (Fig. 7b).  $\text{NO}_x$  was almost diluted to the background level, and net loss of ozone was predicted for the entire altitude range of the simulated plume.

Starting from three days upwind, the plume began to decrease in altitude (Fig. 6d). The CO mixing ratio in the folded results continued to decrease, while ozone mixing ratio increased slightly, with the UFQ of ozone reaching a value of 59 ppbv upon arrival at PMO (Fig. 6a). The dilution observed for CO suggests that the increase in ozone is due to production during subsidence. The decrease in PAN mixing ratio suggests that thermal decomposition of PAN occurred in this stage, which resulted in a 50 % increase in  $\text{NO}_x$  and consequent ozone production (Fig. 6b), a hypothesis that is confirmed by UFQs of ozone production/loss rate. From three to one days upwind, due to a slight increase in ozone production rate in the plume and continued decrease of ozone destruction rate, the net ozone destruction decreased from  $-2.2$  to  $-1 \text{ ppbv day}^{-1}$  (Fig. 6c), and by a half day upwind, the loss rate of ozone was nearly balanced by the production rate. GEOS-Chem profiles for the arrival dates (Fig. 7c and d) indicate that a net ozone production layer (rate of approx.  $1 \text{ ppbv day}^{-1}$ ) with enhanced  $\text{NO}_x$  was present at an altitude of ca. 2 km a.s.l. at 1.8 and 0.8 days upwind, which suggests that a net ozone production layer may have covered a broad upwind area over the central North Atlantic. The concentrated CO layer was actually predicted to be higher in alti-

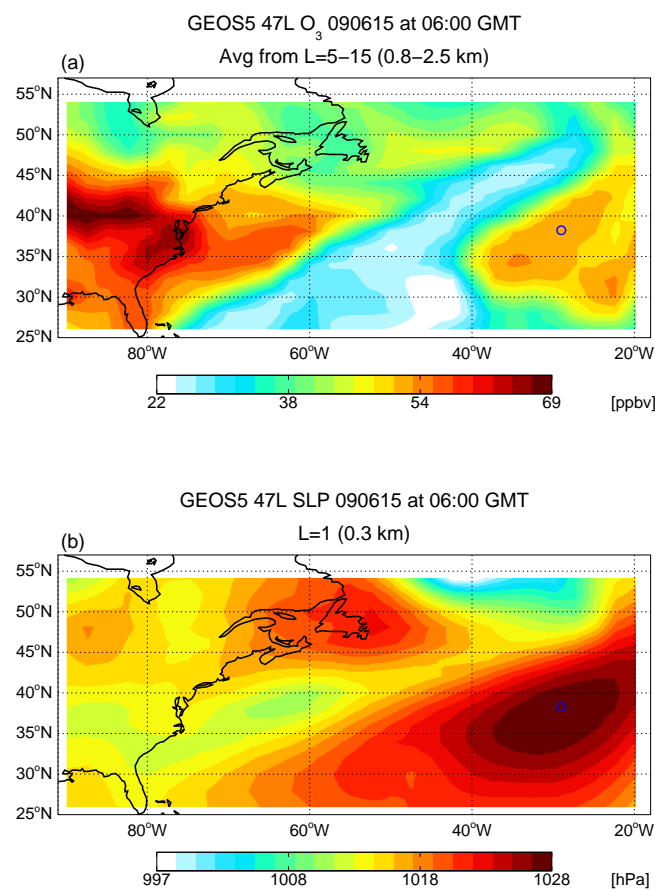


**Fig. 9.** GEOS-Chem-simulated ozone mixing ratio averaged from 0.8 to 2.5 km altitude (**a**) and surface pressure (**b**) at the arrival time of event 2 (15 June 2009, 06:00 UTC). The location of Pico Mountain Observatory is indicated with a blue circle.

tude than the layers in which  $\text{NO}_x$  and ozone production rates were elevated, which suggests that net ozone production occurred more efficiently in the lower portion of the pollution plume where PAN decomposed as a result of higher temperature.

To demonstrate the link between plume subsidence and the Azores–Bermuda High (ABH), we show a plan view of averaged  $\text{O}_3$  in the lower FT (0.8–2.5 km) and surface pressure over the North Atlantic at the time when the plume arrived at PMO (Fig. 9). This GEOS-Chem simulation result indicates that ozone was abundant over the U.S. and southern Canada due to large anthropogenic emissions, as well as in the region impacted by direct transport from the continent, extending several hundred kilometers to the North Atlantic. An ozone-rich region was also present over the Azores region, isolated from the other regions of enhanced ozone, similar to findings presented by Creilson et al. (2003). We conclude that the region of elevated ozone was a result of subsidence, discussed above. Indeed, the position and shape of the ABH correlates well with the ozone-rich region over the Azores, providing

an explanation for air mass subsidence (ABH system) and associated PAN decomposition.

#### 4.2 Event 6 (16–21 July 2010)

A similar analysis was carried out for event 6. The UFQs for event 6 are shown in Fig. 6e–h, and profiles at four upwind times are presented in Fig. 8. The plume associated with event 6 was characterized by low-altitude transport, as described in Sect. 3.2. Six to five days upwind, the plume was located in the PBL over the mid-eastern U.S. (Fig. 3c). The plume contained high levels of CO and ozone (98 ppbv and 70 ppbv, respectively), and an  $O_3$  production rate of 3–6 ppbv day $^{-1}$  ( $PO_x = 13\text{--}17$  and  $LO_x = 10\text{--}11$  ppbv day $^{-1}$ ) prior to export. This  $O_3$  production rate is larger than that observed for event 2 (2.5 ppbv day $^{-1}$ ). In contrast to event 2, stable weather conditions were observed at this time over the eastern U.S. Air masses with fresh pollution emissions were well mixed, and stagnant atmospheric conditions were favorable for ozone production (Jacob et al., 1993). Simulated  $NO_x$  from lightning also showed a maximum prior to plume export. The predicted amount of  $NO_x$  produced was less than 10 % of the total  $NO_x$  UFQs in the simulated plume. This amount was not significant enough to contribute to the simulated ozone production.

From five to four days upwind, the plume was exported to the North Atlantic and traveled mainly at 1–3 km (Fig. 6h), presumably above the MBL, which was predicted to be confined to a layer less than 500 m thick by GEOS-Chem (Fig. 2). UFQs of temperature in the plume were fairly stable and ranged from 280 to 286 K. RH was higher in event 6 (60–80 %) than in event 2 (40–60 %), which indicates a greater part of the event 6 plume may have interacted with a cloud layer during transport and thus was not lifted above the boundary layer. Compared to event 2, these meteorological conditions in the boundary layer may have enhanced destruction of ozone and removal of ozone precursors. Both CO and ozone exhibited a smooth and quick decrease after the simulated plume was exported to the North Atlantic (Fig. 6e). The rate of loss in simulated CO and ozone decreased after three days of transport in the North Atlantic, when concentrations approached background levels. UFQs of nitrogen species in the plume for event 6 also showed similar decreasing trends. In contrast to the PAN accumulation observed in event 2, PAN mixing ratios in this plume decreased following export from the PBL, which implies that the plume lost most of its potential for ozone production. The plume switched from a net ozone production to a net ozone destruction state at four days upwind, and stayed in a net destruction state during the rest of the transport period (Fig. 6g). Net production of ozone decreased during the entire transport and it decreased much more quickly than net ozone loss rate. When the plume arrived at PMO, the plume was in a net ozone destruction state of  $-2$  ppbv day $^{-1}$ . Similar transport in the lower FT was found in a transpacific transport study (Kotchenruther et al.,

2001), as well as in another North American outflow study simulated using WRF-Chem (Lee et al., 2011).

#### 5 Potential causes for enhancement in $d[O_3]/d[CO]$ at PMO

In this section, we analyze observations of  $d[O_3]/d[CO]$  enhancement at PMO and investigate chemical transformation in plumes based on the above findings. We estimate  $d[O_3]/d[CO]$  in the plumes at upwind times for events 2 and 6 by applying estimates of photochemical loss and gain of CO and ozone during transport. We lack in situ measurements of trace gases in the plumes when they were exported from North America. In order to evaluate the values of upwind  $d[O_3]/d[CO]$ , we compare the values to upwind slopes simulated by GEOS-Chem and observational data from the MOZAIC (Measurements of OZone, water vapour, carbon monoxide and nitrogen oxides by in-service Alrbus aircraft) program. The objective of this analysis is to elucidate factors driving variation in  $d[O_3]/d[CO]$  during transport.

##### 5.1 $d[O_3]/d[CO]$ evolution during transport of event 2

For the purpose of this analysis, we assume that the  $d[O_3]/d[CO]$  value obtained by regression of the measurement data is the result of mixing between a so-called “pollution plume point” and background air in the central North Atlantic. Therefore, for event 2, a substitute slope is derived by connecting higher CO and  $O_3$  values in the plume and lower background  $O_3$  and CO values. The plume point for event 2 (red triangle in Fig. 10a) at PMO is determined by averaging the top 10 % of  $O_3$  and CO mixing ratios from measurements associated with this event. The background point is estimated from observed  $O_3$  and CO mixing ratios at PMO during specific periods determined to be representative of the North Atlantic regional background. This determination is made by selecting periods with FLEXPART retroplumes with more than 50 % of their residence time over the North Atlantic region (defined by latitude from 30 to 48°, longitude from  $-60$  to  $-15$ °) and more than 80 % of their residence time under a vertical height of 5 km at 10 days upwind from PMO. Given a typical transport time from North America to PMO is approximately 6–7 days (Honrath et al., 2004), this choice of upwind time insures that the CO and ozone mixing ratios selected were aged midlatitude North Atlantic air. The average CO and  $O_3$  mixing ratios for qualified periods were used as the background point (green circle in Fig. 10a). By connecting the plume point (104 ppbv of CO and 60 ppbv of ozone) and the background point (78 ppbv of CO and 30 ppbv of ozone), a substitute slope (value of 1.15,  $L_1$  in Fig. 10a) for the regression line of observations (value of 1.37,  $L_0$  in Fig. 10a) is obtained. The associated substitute slope can be viewed as a generic  $d[O_3]/d[CO]$  value for event 2 at the central North Atlantic. According to FLEXPART simulation

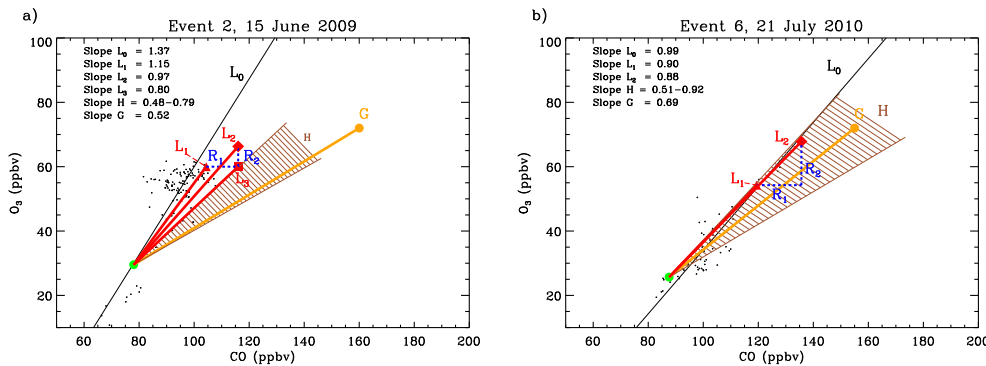


**Fig. 10.** Calculations of  $d[\text{O}_3]/d[\text{CO}]$  for the two selected events (a) event 2 and (b) event 6. Background levels for the central North Atlantic (green circles), and simulated upwind pollution plume data points (red symbols) are defined in the text. Solid black lines ( $L_0$ ) indicate two-sided regression results of observation data (black dots) at PMO. The brown-lined area indicates the  $d[\text{O}_3]/d[\text{CO}]$  range in upwind derived using MOZAIC flight measurements. Line G has an upwind slope that is derived from the GEOS-Chem captured plume. Adjusted lines ( $L_1$ – $L_3$ ) for each event demonstrate the variation in  $d[\text{O}_3]/d[\text{CO}]$  according to chemical transformation pathways ( $R_1$ – $R_2$ ) during transport.

results, transport from tropical regions occurred immediately after this event, so a few observations of clean air (Fig. 10a) were included in the event period.

To derive the upwind slope values of the plume for event 2, we estimate CO and  $\text{O}_3$  mixing ratios in the plume at five days upwind (near the coast) based on folded results from Sect. 4. As previously discussed, transport of event 2 is characterized by initial lifting from PBL into the free troposphere and subsequent subsidence near PMO. Since CO transformation is less affected by transport height and temperature, we begin by estimating the upwind CO mixing ratio in the plume by calculating CO production and CO loss over the transport time. By knowing the production/loss rate of CO in the folded results, we calculate the percent production/loss relative to CO mixing ratio in the folded results for each day. For example, if the CO net destruction rate were  $-1.16 \text{ ppb day}^{-1}$  ( $PCO = 1.25$  and  $LCO = 2.41 \text{ ppb day}^{-1}$ ), we compute a 1.4 % loss relative to an average CO mixing ratio of 85 ppbv during the last day of transport. By doing this computation iteratively for each day, we obtain a total loss of 10 % of CO during five days of transport. To compare this net CO loss with values found by Honrath et al. (2004), we can compute the CO loss based on reaction with OH, and CO production based on oxidation of hydrocarbons. By applying an average OH concentration of  $2.8 \times 10^6 \text{ molecules cm}^{-3}$ , Honrath et al. (2004) estimated a 23–27 % CO loss due to reaction with OH during 5–6 days of transport from the east coast of the U.S. to PMO. The average OH concentration estimated in our folded results was  $3.0 \times 10^6 \text{ molecules cm}^{-3}$ , which gives a 25 % loss of CO by reaction with OH in the five days of transport. Considering that in the folded results, the predicted CO production rate from the oxidation of hydrocarbons is about half of the CO destruction rate, a net loss of CO of 13 % is expected, consistent with the estimation of CO loss calculated iteratively

of 10 %. According to an estimated 10 % loss of CO, we expect the plume point (red triangle in Fig. 10a) to move to the right to a CO level of 116 ppbv at five days upwind following process  $R_1$ . By using the same iterative calculation of relative ozone production/loss for each day, we compute an 11 % loss in ozone for the transport period, moving the plume point (following  $R_2$  in Fig. 10a) up to an ozone level of 66 ppbv (red diamond in Fig. 10a). The slope of the line ( $L_2$  in Fig. 10a) connecting this upwind plume point and the background point, which is presumably unchanged, is 0.97. Comparing  $L_1$  and  $L_2$ , we conclude that both CO and ozone transformation can affect the slope. Net ozone loss has negative contribution to the slope, while net CO loss has positive contribution to the slope. It is also important to note that although the averaged net ozone production rate during the 5-day transport period was negative, the slope increases from  $L_2$  to  $L_1$  as a result of significant CO loss. This finding contradicts the intention of use of  $d[\text{O}_3]/d[\text{CO}]$  as an indicator of net ozone production. To our knowledge, prior to this study, CO loss has been pointed out as a potential explanation for enhancement in  $d[\text{O}_3]/d[\text{CO}]$  only in the study by Real et al. (2008).

In order to evaluate the upwind slope  $L_2$ , we compare it with other estimations of slope values derived from near-coast pollution plumes inferred from our GEOS-Chem simulations. At the time of export from North America (9 June), GEOS-Chem profiles (not shown) indicated that the plume associated with event 2 contained 160 ppbv of CO and 72 ppbv of ozone. If this plume (orange circle in Fig. 10a) were mixed with the background (green circle), the derived upwind slope would be 0.52 (line G).

We also investigated upwind pollution plumes by using flight measurements obtained from the MOZAIC airborne program. To estimate the composition of the event 2 plume when it was exported from eastern North America, we chose

the CO and ozone profiles from Philadelphia, the closest MOZAIC airport to the location of the event origin (see Fig. 3) from 2008 to 2010. The 2008 data were included because there were only a few profiles collected in summertime 2010. CO and ozone mixing ratios measured from an altitude of 2 to 3 km were considered to represent lower free troposphere air. The top 10 % of CO mixing ratios at this level were treated as highly polluted air and were used to determine the potential range of the initial plume conditions for event 2. By connecting these CO and ozone mixing ratios in the plume with the North Atlantic background, we obtained a range in upwind  $d[\text{O}_3]/d[\text{CO}]$  from 0.48 to 0.79 (H range in Fig. 10a). This range is a little larger than those of recent satellite observations downwind of eastern North America (0.4–0.6; Voulgarakis et al., 2011), but consistent with values measured near coastal areas observed during the ICARTT Campaign (0.81 and 0.72; Zhang et al., 2006).

Compared to the slope range of the G and H lines, the upwind slope for event 2 based on the folded results (1.15 for  $L_2$ ) is greater than the upper end of the slope range of G and H lines and is probably overestimated. We speculate that our calculation of ozone transformation during transport in event 2 underestimated net ozone production during plume subsidence, which is likely caused by numerical diffusion in GEOS-Chem. Due to retention of  $\text{NO}_x$  in the PAN chemical reservoir during rapid lifting from the PBL and subsequent transport at high altitude ( $> 3 \text{ km}$ ), the plume had a potential for ozone production during subsidence in the last two days of transport as PAN decomposed to  $\text{NO}_x$ . This sequence of events, including net ozone production during plume subsidence, occurred in a limited space. However, the  $\text{NO}_x$  generated was immediately diluted in GEOS-Chem grid cells as a result of numerical diffusion, and as a result, net ozone production within the plume would be underestimated in GEOS-Chem simulations and associated folding calculations. As discussed in Sect. 3, the pollution plume for event 2 was compact during transport, as such was vulnerable to numerical diffusion, which may have amplified the underestimation of  $\text{NO}_x$  and net ozone production in the plume. This artifact can be minimized by using higher-resolution chemical models, which reduces the magnitude of artificial mixing with the ambient air. If we assume a hypothetical, averaged, net ozone production rate of  $2.1 \text{ ppbv day}^{-1}$  (7.2 % net ozone production) during the last two days of transport instead of the simulated, averaged, net ozone destruction rate of  $-0.6 \text{ ppbv day}^{-1}$  (3.7 % net ozone loss averaged from the folded result values on upwind days 2 and 1; Fig. 6c), there would be no accumulated ozone change (0 % net ozone production) for the 5-day transport period because the net ozone loss in the first three days would be compensated for by this hypothetical higher net ozone production rate. In this case, the upwind plume point for event 2 would remain at an ozone level of 60 ppbv (red square in Fig. 10a), producing an upwind slope of 0.80 as shown in Fig. 10a for  $L_3$ , instead of ozone being increased at five days upwind to account for

ozone destruction predicted in the folded result ( $R_2$ ; slope of  $L_2 = 0.97$ ). Compared with  $L_2$ , the slope of  $L_3$  shows better agreement with the upwind slopes of lines G and H, which means that the net ozone production was likely closer to the assumed value ( $2.1 \text{ ppbv day}^{-1}$ ) in the final two days of transport. In the remote North Atlantic, this ozone production rate is possible because of the considerably higher ozone production efficiency resulting from fresh  $\text{NO}_x$  production. Based on aircraft measurement of  $\text{NO}_x$  in the FT, Reeves et al. (2002) calculated a pollution plume with a net ozone production rate of  $9.6 \text{ ppbv day}^{-1}$  with a simultaneously measured NO value  $> 60 \text{ pptv}$ . When the plume was lifted, GEOS-Chem and the folded results could similarly underestimate PAN accumulation due to numerical diffusion, which would also result in underestimation of net ozone production during subsequent subsidence. Correction for this underestimation could move the slope of  $L_3$  even lower and closer to the G and H lines.

If the explanation that GEOS-Chem underestimates instantaneous ozone production is correct, enhancement of  $d[\text{O}_3]/d[\text{CO}]$  in event 2 (from  $L_3$  to  $L_1$  in Fig. 10a) was the result of a combination of ozone production and CO loss during transport. Compared to upwind CO and ozone mixing ratios in the upwind plume simulated in GEOS-Chem (orange circle), the upwind CO and ozone mixing ratios calculated above (red square on  $L_3$ ) are much lower. This discrepancy is a result of our calculation based on diluted pollution plumes observed at PMO. However, the dilution effect, i.e., mixing, does not change the slope values because mixing of the pollution plume with background air would only move the plume point along the derived slope line ( $L_3$ ) in a direction opposite to the background point.

## 5.2 $d[\text{O}_3]/d[\text{CO}]$ evolution during transport of event 6

The evolution of  $d[\text{O}_3]/d[\text{CO}]$  in event 6 can be studied using a similar approach (Fig. 10b). Averaging the top 10 % of CO and ozone mixing ratios for the data observed for event 6 produces a computed plume point of 119 ppbv CO and 54 ppbv ozone at the arrival time (red triangle in Fig. 10b). Similarly, the North Atlantic background CO and ozone for summertime 2010 were found to be 88 ppbv and 26 ppbv, respectively (green circle in Fig. 10b). The derived line connecting these two points exhibits a slope of 0.90 ( $L_1$  in Fig. 10b) as a substitute for the regression slope for event 6 (0.99;  $L_0$ ).

According to the folded results, both CO and ozone concentration decreased during transport, and no net ozone production was found, so we expect the plume point for event 6 to move to the upper right in Fig. 10b when tracing back five days upwind. By using the same approach for event 2, we estimate 12 % CO loss during transport for event 6, more loss than in event 2 due to higher OH levels in the plume ( $4.5 \times 10^6 \text{ molecules cm}^{-3}$  daily average value from GEOS-Chem), which may be a result of more efficient ozone

production and export at lower altitude. This CO loss moves the plume point horizontally to the right in Fig. 10b (following  $R_1$ ). Similarly, we estimate 20 % ozone loss during the entire five days of transport. By adjusting for loss of CO ( $R_1$  in Fig. 10b) and of ozone ( $R_2$ ), the plume point is moved to 136 ppbv CO and 68 ppbv ozone for five days earlier (red diamond in Fig. 10b), which, when connected to the background point, produces an upwind slope of 0.88 ( $L_2$ ). Similarly, we estimate upwind slopes by using GEOS-Chem simulation and plumes observed during previous aircraft campaigns. An upwind plume associated with event 6, with 155 ppbv of CO and 72 ppbv of  $O_3$ , was captured by GEOS-Chem five days upwind. Thus, a value of 0.69 is computed as the upwind slope based on the GEOS-Chem simulation (line G). We also estimated the CO and ozone composition for event 6 plume when it was exported from North America by using the same approach as for event 2. Profiles from Atlanta were used because it was the closest MOZAIC airport to the location of export in event 6. By connecting the estimated CO and ozone composition and the background point, we obtained a range of upwind  $d[O_3]/d[CO]$  from 0.51 to 0.92 (H range in Fig. 10b).

The derived upwind slope of line  $L_2$  (0.88) is very close to the slope of  $L_1$  (0.90). Far away from continental pollution sources, the plume for event 6 lost most  $NO_x$  and PAN for net ozone production after export. As a result, significant ozone loss occurred in transport to PMO, which resulted in a negative contribution to  $d[O_3]/d[CO]$ . However, this negative contribution was partially compensated for by significant CO loss during transport. Therefore, the downwind slope (of  $L_1$ ) has a similar value to the slope of  $L_2$ . Both  $L_1$  and  $L_2$  slopes fall in the range of the estimated upwind slopes (slopes of G and H lines ranging from 0.51 to 0.92), which suggests a low variation in  $d[O_3]/d[CO]$  during transport for event 6. Different from event 2, for event 6, numerical diffusion in GEOS-Chem had a minor effect on estimated CO; ozone production/loss because chemical transformation was more continuous; and intensive and abrupt chemical processes, such as net ozone production during subsidence, were absent. The over-dilution caused by numerical diffusion has less a significant effect in event 6 than in event 2 because the plume for event 6 experienced more efficient mixing during transport. This type of mixing is better approximated as numerical diffusion in GEOS-Chem as compared to the mixing during transport associated with event 2 discussed above. As a result, better agreement between the estimated upwind event plume point (red diamond, Fig. 10b) and the adjusted simulated and previously observed plume points (upper end of G and H lines) is observed.

Usually, net ozone production is believed to be the reason for  $d[O_3]/d[CO]$  enhancement in remote regions (Parish et al., 1993). Here we observed that variation in  $d[O_3]/d[CO]$  is not sufficiently explained by net ozone production/loss alone, as previously suggested by Voulgarakis et al. (2011). Instead, significant CO loss during the

two transport events was found to contribute to increases in  $d[O_3]/d[CO]$ . As a result of sufficient ozone export in the two event plumes, high OH concentrations were found in our simulation results ( $3.0 \times 10^6$  molecules  $cm^{-3}$  for event 2;  $4.5 \times 10^6$  molecules  $cm^{-3}$  for event 6 as diurnal average during the transport period) in comparison with typical background OH levels of approximately  $1.0 \times 10^6$  molecules  $cm^{-3}$ . Elevation in OH level, caused by high ozone concentration in the plumes, in turn accelerates CO oxidation, which suggests that use of CO as an inert gas tracer of pollution events in the analysis of  $d[O_3]/d[CO]$  in pollution plumes is biased by a contribution from significant loss of CO.

## 6 Conclusions

We used measurements of atmospheric tracer gases at PMO, the transport model FLEXPART, and the chemical transport model GEOS-Chem to identify transport events that were mainly impacted by North American anthropogenic emissions in the summers of 2009 and 2010. Both FLEXPART and GEOS-Chem were able to simulate the transport processes of the two selected events, and the agreement between the two model simulations of plume transport dynamics allowed us to examine the aging and chemical transformations occurring in the plume with a semi-Lagrangian framework.

CO enhancement observed at PMO was used as a primary indicator of the impact of pollution plumes. Correlation coefficients of  $d[O_3]/d[CO]$  for selected events show significant enhancement in pollution-impacted measurements, and regression analyses of  $d[O_3]/d[CO]$  in selected plumes exhibit high correlation ( $R^2 > 0.5$ ). We successfully identified two North American anthropogenic pollution plumes by examining CO sources, trajectory analyses, and excluding influence of mechanically forced upslope flow to the observatory. The folded GEOS-Chem and FLEXPART technique was applied to study chemical evolution in the two selected events. Lagrangian information including plume dispersion and transport in FLEXPART were used to extract chemical transformation information in GEOS-Chem Eulerian fields. Although the accuracy of the folded results is likely limited by numerical diffusion in GEOS-Chem and transport discrepancy between the models, these results indicate that meteorological conditions and transport pathways largely determined the chemical transformation in the pollution plumes. Based on these analyses, two parameters – transport height and concentration of hydroxyl radical – are important determinants of production and loss of air pollutants during transport over the North Atlantic. For example, our results lead us to conclude that  $NO_x$  was converted into PAN during quick lifting into the middle free troposphere in the beginning of event 2, while most of the reactive nitrogen species were lost to deposition at low altitude in event 6. Exported plumes are usually transported directly from the northeastern

U.S., followed by looping south to intercept PMO. During event 2 in 2009, the plume experienced pronounced subsidence caused by the ABH when approaching the observatory. NO<sub>x</sub> released through thermal decomposition of PAN created a net ozone production layer at 2 km a.s.l. in the Azores. For event 6, the potential for ozone production was low due to active mixing at low altitude, and ozone was primarily destroyed during transport. The enhancement in  $d[\text{O}_3]/d[\text{CO}]$  for event 6 was instead the result of efficient CO loss during transport. High ozone and OH levels in the pollution plumes accelerated CO loss, which brings into question the validity of assuming CO to be a conserved passive tracer of pollution plumes. We conclude that enhanced  $d[\text{O}_3]/d[\text{CO}]$  values, which have been frequently used as indicators of ozone production in transport plumes, may not reflect ozone chemistry only. CO destruction in the plume can also explain the higher  $d[\text{O}_3]/d[\text{CO}]$  observed for event 2, when both CO loss and ozone production were identified.

**Acknowledgements.** Mike Dziobak (Michigan Technological University), Jacques Hueber (University of Colorado), and Paulo Fialho (University of the Azores) helped with logistics and operation of measurements at the Pico Mountain Observatory. This study was supported by U.S. National Science Foundation award no. ATM-0720955. The Leverhulme Trust also provided financial support for this work. S. Wu and A. Kumar acknowledge funding from the U.S. EPA STAR program (grant no. 83518901). Research at the Pico Mountain Observatory has also been supported with funding from the UK National Environment Research Council, administered through the University of Edinburgh, and the Regional Government of the Azores. The authors acknowledge the European Commission for the support to the MOZAIC project (1994–2003) and the preparatory phase of IAGOS (2005–2012). The authors also thank all scientists involved in the program and Valérie Thouret's help in getting access to the data.

Edited by: S. Matthiesen

## References

- Auvray, M. and Bey, I.: Long-range transport to Europe: Seasonal variations and implications for the European ozone budget, *J. Geophys. Res.*, 110, D11303, doi:10.1029/2004JD005503, 2005.
- Auvray, M., Bey, I., Llull, E., Schultz, M. G., and Rast, S.: A model investigation of tropospheric ozone chemical tendencies in long-range transported pollution plumes, *J. Geophys. Res.*, 112, D05304, doi:10.1029/2006JD007137, 2007.
- Ayers, G. P.: Comment on regression analysis of air quality data, *Atmos. Environ.*, 35, 2423–2425, doi:10.1016/S1352-2310(00)00527-6, 2001.
- Berkowitz, C. M., Daum, P. H., Spicer, C. W., and Busness, K. M.: Synoptic patterns associated with the flux of excess ozone to the western north atlantic, *J. Geophys. Res.*, 101, 28923–28933, doi:10.1029/95JD03274, 1996.
- Bey, I., Jacob, D. J., Yantosca, R. M., Logan, J. A., Field, B. D., Fiore, A. M., Li, Q. B., Liu, H. G. Y., Mickley, L. J., and Schultz, M. G.: Global modeling of tropospheric chemistry with assimilated meteorology: model description and evaluation, *J. Geophys. Res.*, 106, 23073–23095, doi:10.1029/2001JD000807, 2001.
- Charles, J.: Matrix Theory and Applications, the American Mathematical Society, Phoenix, Arizona, USA, 87–170, 1989.
- Chameides, W. L., Fehsenfeld, F., Rodgers, M. O., Cardelino, C., Martinez, J., Parrish, D., Lonneman, W., Lawson, D. R., Rasmussen, R. A., Zimmerman, P., Greenberg, J., Middleton, P., and Wang, T.: Ozone precursor relationships in the ambient atmosphere, *J. Geophys. Res.*, 97, 6037–6055, doi:10.1029/91JD03014, 1992.
- Chin, M., Jacob, D. J., Munger, J. W., Parrish, D. D., and Doddrige, B. G.: Relationship of ozone and carbon-monoxide over north-america, *J. Geophys. Res.*, 99, 14565–14573, doi:10.1029/94JD00907, 1994.
- Cooper, O. R., Moody, J. L., Thornberry, T. D., Town, M. S., and Carroll, M. A.: Prophet 1998 meteorological overview and air-mass classification, *J. Geophys. Res.*, 106(D20), 24289–24299, doi:10.1029/2000JD900409, 2001.
- Creilson, J. K., Fishman, J., and Wozniak, A. E.: Intercontinental transport of tropospheric ozone: a study of its seasonal variability across the North Atlantic utilizing tropospheric ozone residuals and its relationship to the North Atlantic Oscillation, *Atmos. Chem. Phys.*, 3, 2053–2066, doi:10.5194/acp-3-2053-2003, 2003.
- Daum, P. H., Kleinman, L. I., Newman, L., Luke, W. T., WeinsteinLloyd, J., Berkowitz, C. M., and Busness, K. M.: Chemical and physical properties of plumes of anthropogenic pollutants transported over the North Atlantic during the North Atlantic Regional Experiment, *J. Geophys. Res.*, 101, 29029–29042, doi:10.1029/95JD03163, 1996.
- Davis, S. R., Talbot, R., and Mao, H.: Transport and outflow to the North Atlantic in the lower marine troposphere during ICARTT 2004, *Atmos. Chem. Phys. Discuss.*, 12, 2395–2434, doi:10.5194/acpd-12-2395-2012, 2012.
- DeCaria, A. J., Pickering, K. E., Stenchikov, G. L., and Ott, L. E.: Lightning-generated NO<sub>x</sub> and its impact on tropospheric ozone production: a three-dimensional modeling study of a Stratosphere-Troposphere Experiment: Radiation, Aerosols and Ozone (STERAO-A) thunderstorm, *J. Geophys. Res.*, 110, D14303, doi:10.1029/2004JD005556, 2005.
- Duncan, B. N., Logan, J. A., Bey, I., Megretskaia, I. A., Yantosca, R. M., Novelli, P. C., Jones, N. B., and Rinsland, C. P.: Global budget of CO, 1988–1997: Source estimates and validation with a global model, *J. Geophys. Res.*, 112, D22301, doi:10.1029/2007JD008459, 2007.
- Evans, M. and Jacob, D.: Impact of new laboratory studies of N<sub>2</sub>O<sub>5</sub> hydrolysis on global model budgets of tropospheric nitrogen oxides, ozone, and OH, *Geophys. Res. Lett.*, 32, doi:10.1029/2005GL022469, 2005.
- Fehsenfeld, F. C., Daum, P., Leaitch, W. R., Trainer, M., Parrish, D. D., and Hubler, G.: Transport and processing of O<sub>3</sub> and O<sub>3</sub> precursors over the North Atlantic: an overview of the 1993 North Atlantic Regional Experiment (NARE) summer intensive, *J. Geophys. Res.*, 101, 28877–28891, doi:10.1029/2006JD007829, 1996.
- Fehsenfeld, F. C., Ancellet, G., Bates, T. S., Goldstein, A. H., Hardisty, R. M., Honrath, R., Law, K. S., Lewis, A. C., Leaitch, R.,

- McKeen, S., Meagher, J., Parrish, D. D., Pszenny, A. A. P., Russell, P. B., Schlager, H., Seinfeld, J., Talbot, R., and Zbinden, R.: International Consortium for Atmospheric Research on Transport and Transformation (ICARTT): North America to Europe – overview of the 2004 summer field study, *J. Geophys. Res.*, 111, D23S01, doi:10.1029/2006JD007829, 2006.
- Fischer, E. V., Jaffe, D. A., and Weatherhead, E. C.: Free tropospheric peroxyacetyl nitrate (PAN) and ozone at Mount Bachelor: potential causes of variability and timescale for trend detection, *Atmos. Chem. Phys.*, 11, 5641–5654, doi:10.5194/acp-11-5641-2011, 2011.
- Fishman, J. and Seiler, W.: Correlative nature of ozone and carbon monoxide in the troposphere: implications for the tropospheric ozone budget, *J. Geophys. Res.*, 88, 3662–3670, doi:10.1029/JC088iC06p03662, 1983.
- Guerova, G., Bey, I., Attié, J.-L., Martin, R. V., Cui, J., and Sprenger, M.: Impact of transatlantic transport episodes on summertime ozone in Europe, *Atmos. Chem. Phys.*, 6, 2057–2072, doi:10.5194/acp-6-2057-2006, 2006.
- Hegarty, J., Mao, H., and Talbot, R.: Synoptic influences on springtime tropospheric O<sub>3</sub> and CO over the North American export region observed by TES, *Atmos. Chem. Phys.*, 9, 3755–3776, doi:10.5194/acp-9-3755-2009, 2009.
- Helmlig, D., Tanner, D. M., Honrath, R. E., Owen, R. C., and Parrish, D. D.: Nonmethane hydrocarbons at Pico Mountain, Azores: 1. Oxidation chemistry in the North Atlantic region, *J. Geophys. Res.*, 113, D20S91, doi:10.1029/2007JD008930, 2008
- Honrath, R. E., Owen, R. C., Val Martin, M., Reid, J. S., Lapina, K., Fialho, P., Dziobak, M. P., Kleissl, J., and Westphal, D. L.: Regional and hemispheric impacts of anthropogenic and biomass burning emissions on summertime CO and O<sub>3</sub> in the North Atlantic lower free troposphere, *J. Geophys. Res.*, 109, D24310, doi:10.1029/2004JD005147, 2004.
- Honrath, R. E., Helmlig, D., Owen, R. C., Parrish, D. D., and Tanner, D. M.: Nonmethane hydrocarbons at Pico Mountain, Azores: 2. Event-specific analyses of the impacts of mixing and photochemistry on hydrocarbon ratios, *J. Geophys. Res.*, 113, D20S92, doi:10.1029/2008JD009832, 2008.
- Huang, Y., Wu, S., Dubey, M. K., and French, N. H. F.: Impact of aging mechanism on model simulated carbonaceous aerosols, *Atmos. Chem. Phys.*, 13, 6329–6343, doi:10.5194/acp-13-6329-2013, 2013.
- Hudman, R. C., Jacob, D. J., Turquety, S., Leibensperger, E. M., Murray, L. T., Wu, S., Gilliland, A. B., Avery, M., Bertram, T. H., Brune, W., Cohen, R. C., Dibb, J. E., Flocke, F. M., Fried, A., Holloway, J., Neuman, J. A., Orville, R., Perring, A., Ren, X., Sachse, G. W., Singh, H. B., Swanson, A., and Wooldridge, P. J.: Surface and lightning sources of nitrogen oxides over the United States: Magnitudes, chemical evolution, and outflow, *J. Geophys. Res.*, 112, D12S05, doi:10.1029/2006JD007912, 2007.
- Hudman, R. C., Murray, L. T., Jacob, D. J., Turquety, S., Wu, S., Millet, D. B., Avery, M., Goldstein, A. H., and Holloway, J.: North American influence on tropospheric ozone and the effects of recent emission reductions: Constraints from ICARTT observations, *J. Geophys. Res.*, 114, D07302, doi:10.1029/2008JD010126, 2009.
- Jacob, D. J., Logan, J. A., Yevich, R. M., Gardner, G. M., Spivakovskiy, C. M., Wofsy, S. C., Munger, J. W., Silliman, S., Prather, M. J., Rodgers, M. O., Westberg, H., and Zimmerman, P. R.: Simulation of summertime ozone over North America, *J. Geophys. Res.*, 98, 14797–14816, doi:10.1029/93JD01223, 1993.
- Jacobson, M. Z. and Turco, R. P.: SMVGEAR: a sparse-matrix, vectorized Gear code for atmospheric models, *Atmos. Environ.*, 28, 273–284, 1994.
- Kleindienst, T. E.: Recent developments in the chemistry and biology of peroxyacetyl nitrate, *Res. Chem. Intermediat.*, 20, 335–384, doi:10.1163/156856794X00379, 1994.
- Kleissl, J., Honrath, R. E., Dziobak, M. P., Tanner, D., Martin, M. V., Owen, R. C., and Helmlig, D.: Occurrence of upslope flows at the Pico mountaintop observatory: A case study of orographic flows on a small, volcanic island, *J. Geophys. Res.*, 112, D10S35, doi:10.1029/2006JD007565, 2007.
- Kotchenruther, R. A., Jaffe, D. A., and Jaegle, L.: Ozone photochemistry and the role of peroxyacetyl nitrate in the springtime northeastern Pacific troposphere: results from the Photochemical Ozone Budget of the Eastern North Pacific Atmosphere (PHOBEA) campaign, *J. Geophys. Res.*, 106, 28731–28742, doi:10.1029/2000JD000060, 2001.
- Kumar, A., Wu, S., Weise, M. F., Honrath, R., Owen, R. C., Helmlig, D., Kramer, L., Val Martin, M., and Li, Q.: Free-troposphere ozone and carbon monoxide over the North Atlantic for 2001–2011, *Atmos. Chem. Phys.*, 13, 12537–12547, doi:10.5194/acp-13-12537-2013, 2013.
- Lapina, K., Honrath, R. E., Owen, R. C., Martin, M. V., and Pfister, G.: Evidence of significant large-scale impacts of boreal fires on ozone levels in the midlatitude Northern Hemisphere free troposphere, *Geophys. Res. Lett.*, 33, L10815, doi:10.1029/2006GL025878, 2006.
- Lee, S.-H., Kim, S.-W., Trainer, M., Frost, G. J., McKeen, S. A., Cooper, O. R., Flocke, F., Holloway, J. S., Neuman, J. A., Ryerson, T., Senff, C. J., Swanson, A. L., and Thompson, A. M.: Modeling ozone plumes observed downwind of New York City over the North Atlantic Ocean during the ICARTT field campaign, *Atmos. Chem. Phys.*, 11, 7375–7397, doi:10.5194/acp-11-7375-2011, 2011.
- Li, Q., Jacob, D. J., Munger, J. W., Yantosca, R. M., and Parrish, D. D.: Export of NO<sub>x</sub> from the north american boundary layer: Reconciling aircraft observations and global model budgets, *J. Geophys. Res.*, 109, D02313, doi:10.1029/2003JD004086, 2004.
- Li, Q., Jacob, D. J., Park, R., Wang, Y., Heald, C. L., Hudman, R., Yantosca, R. M., Martin, R. V., and Evans, M.: North american pollution outflow and the trapping of convectively lifted pollution by upper-level anticyclone, *J. Geophys. Res.*, 110, D10301, doi:10.1029/2004JD005039, 2005.
- Liang, J., Horowitz, L. W., Jacob, D. J., Wang, Y. H., Fiore, A. M., Logan, J. A., Gardner, G. M., and Munger, J. W.: Seasonal budgets of reactive nitrogen species and ozone over the united states, and export fluxes to the global atmosphere, *J. Geophys. Res.*, 103, 13435–13450, doi:10.1029/97JD03126, 1998.
- Liu, S. C., Trainer, M., Fehsenfeld, F. C., Parrish, D. D., Williams, E. J., Fahey, D. W., Hubler, G., and Murphy, P. C.: Ozone production in the rural troposphere and the implications for regional and global ozone distributions, *J. Geophys. Res.*, 92, 4191–4207, 1987.
- Logan, J. A., Prather, M. J., Wofsy, S. C., and McElroy, M. B.: Tropospheric chemistry – a global perspective, *J. Geophys. Res. Oc. Atmos.*, 86(NC8), 7210–7254, 1981.

- Martin, R. V., Jacob, D. J., Logan, J. A., Bey, I., Yantosca, R. M., Staudt, A. C., Li, Q., Fiore, A. M., Duncan, B. N., Liu, H., Ginoux, P., and Thouret, V.: Interpretation of TOMS observations of tropical tropospheric ozone with a global model and in situ observations, *J. Geophys. Res.*, 107, 2156–2202, doi:10.1029/2001JD001480, 2002.
- Mahlman, J. D., Levy, H., and Moxim, W. J.: 3-dimensional tracer structure and behavior as simulated in 2 ozone precursor experiments, *J. Atmos. Sci.*, 37, 655–685, 1980.
- Mao, H., Talbot, R., Troop, D., Johnson, R., Businger, S., and Thompson, A. M.: Smart balloon observations over the North Atlantic: O<sub>3</sub> data analysis and modeling, *J. Geophys. Res.*, 111, D23S56, doi:10.1029/2005JD006507, 2006.
- McKeen, S. A. and Liu, S. C.: Hydrocarbon ratios and photochemical history of air masses, *Geophys. Res. Lett.*, 20, 2363–2366, doi:10.1029/93GL02527, 1993.
- Methven, J., Arnold, S. R., Stohl, A., Evans, M. J., Avery, M., Law, K., Lewis, A. C., Monks, P. S., Parrish, D. D., Reeves, C. E., Schlager, H., Atlas, E., Blake, D. R., Coe, H., Crosier, J., Flocke, F. M., Holloway, J. S., Hopkins, J. R., McQuaid, J., Purvis, R., Rappenglück, B., Singh, H. B., Watson, N. M., Whalley, L. K., and Williams, P. I.: Establishing Lagrangian connections between observations within air masses crossing the Atlantic during the International Consortium for Atmospheric Research on Transport and Transformation experiment, *J. Geophys. Res.*, 111, D23S62, doi:10.1029/2006JD007540, 2006.
- Millet, D. B., Goldstein, A. H., Holzinger, R., Williams, B. J., Allan, J. D., Jimenez, J. L., Worsnop, D. R., Roberts, J. M., White, A. B., Hudman, R. C., Bertschi, I. T., and Stohl, A.: Chemical characteristics of north american surface layer outflow: Insights from chebogue point, nova scotia, *J. Geophys. Res.*, 111, D23S53, doi:10.1029/2006JD007287, 2006.
- Mu, M., Randerson, J. T., van der Werf, G. R., Giglio, L., Kasibhatla, P., Morton, D., Collatz, G. J., DeFries, R. S., Hyer, E. J., Prins, E. M., Griffith, D. W. T., Wunch, D., Toon, G. C., Sherlock, V., and Wennberg, P. O.: Daily and 3-hourly variability in global fire emissions and consequences for atmospheric model predictions of carbon monoxide, *J. Geophys. Res.*, 116, D24303, doi:10.1029/2011JD016245, 2011.
- NCAR., Meteorological case study selection kit, <http://www.mmm.ucar.edu/imagearchive/> (last access: November 2013), 2009.
- Neuman, J. A., Parrish, D. D., Trainer, M., Ryerson, T. B., Holloway, J. S., Nowak, J. B., Swanson, A., Flocke, F., Roberts, J. M., Brown, S. S., Stark, H., Sommariva, R., Stohl, A., Peltier, R., Weber, R., Wollny, A. G., Sueper, D. T., Hubler, G., and Fehsenfeld, F. C.: Reactive nitrogen transport and photochemistry in urban plumes over the North Atlantic Ocean, *J. Geophys. Res.*, 111, D23S54, doi:10.1029/2005JD007010, 2006.
- NOAA: US Daily Weather Maps Project, [http://docs.lib.noaa.gov/rescue/dwm/data\\_rescue\\_daily\\_weather\\_maps.html](http://docs.lib.noaa.gov/rescue/dwm/data_rescue_daily_weather_maps.html) (last access: 13 May 2013), 2009.
- Olivier, J. and Berdowski, J.: Global emission sources and sinks, in: The Climate System, A. A. Balkema, Swets & Zeitlinger, the Netherlands, ISBN 9058092550, 33–78, 2001.
- Owen, R. C. and Honrath, R. E.: Technical note: a new method for the Lagrangian tracking of pollution plumes from source to receptor using gridded model output, *Atmos. Chem. Phys.*, 9, 2577–2595, doi:10.5194/acp-9-2577-2009, 2009.
- Owen, R. C., Cooper, O. R., Stohl, A., and Honrath, R. E.: An analysis of the mechanisms of North American pollutant transport to the central North Atlantic lower free troposphere, *J. Geophys. Res.*, 111, D23S58, doi:10.1029/2006JD007062, 2006.
- Parrish, D. D., Hahn, C. J., Williams, E. J., Norton, R. B., Fehsenfeld, F. C., Singh, H. B., Shetter, J. D., Gandrud, B. W., and Ridley, B. A.: Indications of photochemical histories of Pacific air masses from measurements of atmospheric trace species at Point Arena, California, *J. Geophys. Res.*, 97, 15883–15901, 1992.
- Parrish, D. D., Holloway, J. S., Trainer, M., Murphy, P. C., Forbes, G. L., and Fehsenfeld, F. C.: Export of North American ozone pollution to the north Atlantic Ocean, *Science*, 259, 1436–1439, doi:10.1126/science.259.5100.1436, 1993.
- Parrish, D. D., Trainer, M., Holloway, J. S., Yee, J. E., Warshawsky, M. S., Fehsenfeld, F. C., Forbes, G. L., and Moody, J. L.: Relationships between ozone and carbon monoxide at surface sites in the North Atlantic region, *J. Geophys. Res.*, 103, 13357–13376, doi:10.1029/98JD00376, 1998.
- Prados, A. I., Dickerson, R. R., Dodridge, B. G., Milne, P. A., Moody, J. L., and Merrill, J. T.: Transport of ozone and pollutants from north america to the north atlantic ocean during the 1996 atmosphere/ocean chemistry experiment (ae-roce) intensive, *J. Geophys. Res.*, 104(D21), 26219–26233, doi:10.1029/1999JD900444, 1999.
- Real, E., Law, K. S., Schlager, H., Roiger, A., Huntrieser, H., Methven, J., Cain, M., Holloway, J., Neuman, J. A., Ryerson, T., Flocke, F., de Gouw, J., Atlas, E., Donnelly, S., and Parrish, D.: Lagrangian analysis of low altitude anthropogenic plume processing across the North Atlantic, *Atmos. Chem. Phys.*, 8, 7737–7754, doi:10.5194/acp-8-7737-2008, 2008.
- Reeves, C. E., Penkett, S. A., Bauguitte, S., Law, K. S., Evans, M. J., Bandy, B. J., Monks, P. S., Edwards, G. D., Phillips, G., Barjat, H., Kent, J., Dewey, K., Schmitgen, S., and Kley, D.: Potential for photochemical ozone formation in the troposphere over the North Atlantic as derived from aircraft observations during ACSOE, *J. Geophys. Res.*, 107, 4707, doi:10.1029/2002JD002415, 2002.
- Seibert, P. and Frank, A.: Source-receptor matrix calculation with a Lagrangian particle dispersion model in backward mode, *Atmos. Chem. Phys.*, 4, 51–63, doi:10.5194/acp-4-51-2004, 2004.
- Sheppard, P.: Airflow over mountains, *Q. J. Roy. Meteor. Soc.*, 82, 528–529, 1956.
- Stohl, A., Hittenberger, M., and Wotawa, G.: Validation of the Lagrangian particle dispersion model FLEXPART against large-scale tracer experiment data, *Atmos. Environ.*, 32, 4245–4264, doi:10.1016/S1352-2310(98)00184-8, 1998.
- Stohl, A., Eckhardt, S., Forster, C., James, P., and Spichtinger, N.: On the pathways and timescales of intercontinental air pollution transport, *J. Geophys. Res.*, 107, 4684, doi:10.1029/2001JD001396, 2002.
- Streets, D. G., Bond, T. C., Carmichael, G. R., Fernandes, S. D., Fu, Q., He, D., Klimont, Z., Nelson, S. M., Tsai, N. Y., Wang, M. Q., Woo, J.-H., and Yarber, K. F.: An inventory of gaseous and primary aerosol emissions in Asia in the year 2000, *J. Geophys. Res.*, 108, 8809, doi:10.1029/2002JD003093, 2003.
- Thompson, A. M.: The oxidizing capacity of the earths atmosphere – probable past and future changes, *Science*, 256, 1157–1165, 1992.

- Val Martin, M., Honrath, R. E., Owen, R. C., Pfister, G., Fialho, P., and Barata, F.: Significant enhancements of nitrogen oxides, black carbon, and ozone in the North Atlantic lower free troposphere resulting from North American boreal wildfires, *J. Geophys. Res.*, 111, D23S60, doi:10.1029/2006JD007530, 2006.
- Val Martin, M., Honrath, R. E., Owen, R. C., and Li, Q. B.: Seasonal variation of nitrogen oxides in the central North Atlantic lower free troposphere, *J. Geophys. Res.*, 113, D17307, doi:10.1029/2007JD009688, 2008.
- Voulgarakis, A., Telford, P. J., Aghedo, A. M., Braesicke, P., Faluvegi, G., Abraham, N. L., Bowman, K. W., Pyle, J. A., and Shindell, D. T.: Global multi-year O<sub>3</sub>-CO correlation patterns from models and TES satellite observations, *Atmos. Chem. Phys.*, 11, 5819–5838, doi:10.5194/acp-11-5819-2011, 2011.
- Wang, Y., Jacob, D. J., and Logan, J. A.: Global simulation of tropospheric O<sub>3</sub>-NOx-hydrocarbon chemistry 3. origin of tropospheric ozone and effects of nonmethane hydrocarbons. *J. Geophys. Res.*, 103, 10757–10767, 1998.
- Wang, Y., Jacob, D. J., and Logan, J. A.: Global simulation of tropospheric O<sub>3</sub>-NOx-hydrocarbon chemistry 1. Model formulation, *J. Geophys. Res.*, 103, 10713–10725, doi:10.1029/98JD00158, 1998.
- Wang, Y., Jacob, D. J., Sager, P., Streets., D. J., Park, R. J., Gilliland, A. B., and Donkelaar, A.: Surface ozone background in the united states: Canadian and mexican pollution influences, *Atmos. Environ.*, 43, 1310–1319, 2009.
- Weise, M.: Tropospheric ozone and CO over North Atlantic for the past decade, Master's thesis, Michigan Technological University, Houghton, Michigan, USA, 2011.
- Wu, S., Mickley, L. J., Jacob, D. J., Logan, J. A., Yantosca, R. M., and Rind, D.: Why are there large differences between models in global budgets of tropospheric ozone?, *J. Geophys. Res.*, 112, D05302, doi:10.1029/2006JD007801, 2007.
- Wu, S. and Mickley, L. J. and Kaplan, J. O. and Jacob, D. J.: Impacts of changes in land use and land cover on atmospheric chemistry and air quality over the 21st century, *Atmos. Chem. Phys.*, 12, 1597–1609, doi:10.5194/acp-12-1597-2012, 2012.
- Zhang, L., Jacob, D. J., Bowman, K. W., Logan, J. A., Turquety, S., Hudman, R. C., Li, Q., Beer, R., Worden, H. M., Worden, J. R., Rinsland, C. P., Kulawik, S. S., Lampel, M. C., Shephard, M. W., Fisher, B. M., Eldering, A., and Avery, M. A.: Ozone-CO correlations determined by the TES satellite instrument in continental outflow regions, *Geophys. Res. Lett.*, 33, L18804, doi:10.1029/2006GL026399, 2006.
- Zhang, L., Jacob, D. J., Boersma, K. F., Jaffe, D. A., Olson, J. R., Bowman, K. W., Worden, J. R., Thompson, A. M., Avery, M. A., Cohen, R. C., Dibb, J. E., Flock, F. M., Fuelberg, H. E., Huey, L. G., McMillan, W. W., Singh, H. B., and Weinheimer, A. J.: Transpacific transport of ozone pollution and the effect of recent Asian emission increases on air quality in North America: an integrated analysis using satellite, aircraft, ozonesonde, and surface observations, *Atmos. Chem. Phys.*, 8, 6117–6136, doi:10.5194/acp-8-6117-2008, 2008.